

# Forecasting the local progression of the Covid-19 epidemic from medical emergency calls: the example of the Paris area

Stéphane Gaubert<sup>1,2</sup>, Marianne Akian<sup>1,2</sup>, Xavier Allamigeon<sup>1,2</sup>, Marin Boyet<sup>1,2</sup>  
 Baptiste Colin<sup>1,2</sup>, Théotime Grohens<sup>1,3</sup>, Laurent Massoulié<sup>1,4,5</sup>, David P. Parsons<sup>1</sup>  
 Frédéric Adnet<sup>6,7</sup>, Érick Chanzy<sup>6</sup>, Laurent Goix<sup>6</sup>, Frédéric Lapostolle<sup>6,7</sup>  
 Éric Lecarpentier<sup>6</sup>, Christophe Leroy<sup>6</sup>, Thomas Loeb<sup>6</sup>, Jean-Sébastien Marx<sup>6</sup>  
 Caroline Télion<sup>6</sup>, Laurent Tréluyer<sup>6</sup> and Pierre Carli<sup>6,8</sup>

<sup>1</sup> INRIA

<sup>2</sup> CMAP, École polytechnique, IP Paris, CNRS

<sup>3</sup> Université de Lyon, CNRS, INSA-Lyon, LIRIS, UMR5205

<sup>4</sup> ENS, CNRS, PSL University

<sup>5</sup> Microsoft Research-INRIA Joint Centre

<sup>6</sup> AP-HP

<sup>7</sup> Université Paris XIII, Bobigny

<sup>8</sup> Université Paris-Descartes, Paris

Emails: <sup>1</sup>: `Prenom.Nom@inria.fr` <sup>6</sup>: `Prenom.Nom@aphp.fr`

May 28, 2020

**Abstract.** We portray the evolution of the Covid-19 epidemic during the crisis of March-April 2020 in the Paris area, by analyzing the medical emergency calls received by the EMS of the four central departments of this area (Centre 15 of SAMU 75, 92, 93 and 94). Our study reveals strong dissimilarities between these departments. We provide an algorithm, based on a piecewise linear approximation of the logarithm of epidemic observables, allowing one to monitor the epidemic. Our methods combine ideas from several fields of mathematics: tropical geometry, Perron–Frobenius theory, probability and optimization, transport PDE in population dynamics.

**Résumé.** Nous décrivons l'évolution de l'épidémie de Covid-19 dans l'agglomération parisienne, pendant la crise de Mars-Avril 2020, en analysant les appels d'urgence au numéro 15 traités par les SAMU des quatre départements centraux de l'agglomération (75, 92, 93 et 94). Notre étude révèle de fortes disparités entre ces départements. Nous donnons un algorithme, utilisant une approximation linéaire par morceaux du logarithme des observables épidémiques, qui permet de surveiller l'évolution. Nos méthodes sont inspirées par plusieurs domaines des mathématiques: géométrie tropicale, théorie de Perron–Frobenius, probabilités et optimisation, modèles d'EDP de transport en dynamique de population.

# 1 Introduction

The outbreak of Covid-19 in France has put the national Emergency Medical System (EMS), the *SAMU*, in the front line. In the *Île-de-France* region, one most affected by the epidemic, the SAMU centers of Paris and its inner suburbs experienced a major increase in the number of calls received and of the number of ambulance dispatches for Covid-19 patients.

We show that indicators based on EMS calls and vehicle dispatches allow to analyse the evolution of the epidemic. In particular, we show that EMS calls are early signals, allowing one to anticipate vehicle dispatch. We provide a method of short term prediction of the evolution of the epidemic, based on mathematical modelling. This leads to *early detection and early alarm mechanisms* allowing one either to confirm that certain sanitary measures are strong enough to contain the epidemic, or to detect its resurgence. These mechanisms rely on simple data generally available in EMS: numbers of patient records tagged as Covid-19, and among these, numbers of records resulting in medical advice, ambulance dispatch, or Mobile Intensive Care Unit dispatch. We also provide a comparative description of the evolution of the epidemic in the four central departments of the Paris area, showing spatial dissimilarities, including a strong variation of the doubling time, depending on the department.

Our approach relies on several mathematical tools in an essential way. Indeed, the Covid-19 epidemic has unprecedented characteristics, and, given the lack of experience of similar epidemics, one needs to rely on mathematical models. We use transport PDE to represent the dynamics of Covid-19 epidemics. Transport PDE capture epidemics with a significant time interval between contamination and the start of the infectious phase, like Covid-19 (in contrast, ODE models without time delays allow instantaneous transitions to the infectious phase, after contamination). If the majority of the population is susceptible, this dynamics becomes approximately linear and order preserving. Then, it can be analyzed by methods of Perron–Frobenius theory. We show that the logarithm of epidemic observables can be approximated by a piecewise linear map, with as many pieces as there are phases of the epidemic (i.e., periods with different contamination conditions), see Theorem 1. This idea of piecewise linear approximation and of “log glasses”, a key ingredient of the present approach, arises from tropical geometry.

The present work started on March 13<sup>th</sup>, and led to the algorithm presented here. A preliminary version of this algorithm was used, on March 20<sup>th</sup>, to forecast the epidemic wave, anticipating that the peak load of SAMU (which occurred around March 27<sup>th</sup>) would be different depending on the department of the Paris area. We subsequently applied our method to provide Assistance Publique – Hôpitaux de Paris (AP-HP), on April 5<sup>th</sup>, with an early report, quantifying the efficiency of the lockdown measures from the estimation of the contraction rate of the epidemic in the different departments. This algorithm is now deployed operationally in the four SAMU of AP-HP. This work may be quickly reproduced in any EMS.

Although it was developed for Covid-19 and for EMS calls, the present monitoring method is generic. It may also apply to other medical indicators, see Section 3.4, and to other epidemics, for instance, influenza.

This paper is a crisis report, giving a unified picture of a work done jointly by a team of physicians of the SAMU of AP-HP and applied mathematicians from INRIA and École polytechnique. Medical, epidemiological, and mathematical aspects are intricately intertwined in this work. We received help from several physicians, researchers and engineers, not listed as authors, and also help from several organizations. They are thanked in the acknowledgments section.

This paper should also be understood as an announce. The results will be subsequently developed in several papers, with different subsets of coauthors. It is intended to be read both by a medical and a mathematical audience. The first part of the paper, up to Section 6 included, and the conclusion, are intended to a general audience. Mathematical tools are presented in Section 7, Section 8, Section 9 and in the appendix.

The present work shows the epidemiological significance of the calls received by the EMS, it focuses on the mathematical modelling aspects, on the description of the evolution of the epidemic in the Paris area, and on prediction algorithms. The current work<sup>1</sup> with an intersecting set of authors, is coordinated with

---

<sup>1</sup>COVID19 APHP-Universities-INRIA-INSERM, Emergency calls are early indicators of ICU bed requirement during the COVID-19 epidemic, privately circled manuscript, May 2020.

the present one. It focuses on medical aspects. It makes a case study of the Covid-19 crisis of March-April 2020, in Paris, considering the EMS and the hospital services in a unified perspective. It shows that the calls received by SAMU are early predictors of the future load on ICU.

## 2 Context

The mission of the SAMU centers is to provide an appropriate response to calls to the number 15, the French toll-free phone number dedicated to medical emergencies. This service is based on the medical regulation of emergency calls, in the sense that for each patient, a physician decides which response is most appropriate. Thus, depending on the evaluation over the phone of the severity of the case and the circumstances, the response may be a medical advice, a home visit by a general practitioner, the dispatch of a team of EMTs (Emergency Medical Technicians) of either a first aid association or the Fire brigade, or an ambulance of a private company. A Mobile Intensive Care Unit (MICU), staffed by a physician, a nurse and an EMT, is sent to the scene as a second or a first tier, when a life threatening problem is suspected. The role of the SAMU in the management of disasters or mass casualties has been described elsewhere [12, 2]. The city of Paris and its inner suburbs are covered by 4 departmental SAMU Center-15 : Paris (75), Hauts-de-Seine (92), Seine Saint-Denis (93), and Val-de-Marne (94). They serve a population of 6.77 million inhabitants. These four Center-15 are part of the public hospital administration, AP-HP (Assistance Publique – Hôpitaux de Paris). They operate identically and use the same computerized call management system. Since the outbreak of the Covid-19 epidemic, the French government instructed the public that anyone with signs of respiratory infection or fever should not go directly to the hospital emergency room to limit overcrowding, but should call number 15 for orientation. To comply with the recommendations of the health care authorities, the four Center-15 applied the same procedures: after medical call regulation, only patients with signs of severity or significant risk factors were transported by EMTs and ambulances to hospitals, either to Emergency Room (ER) or newly created Covid-19 Units. The cases presenting a life-threatening emergency, mostly respiratory distress, were managed by an MICU team and then admitted directly in Intensive Care Unit (ICU). All other cases were advised to stay at home and isolate themselves. When necessary, these patients were also eligible for a home visit by a general practitioner or a consultation appointment the following days.

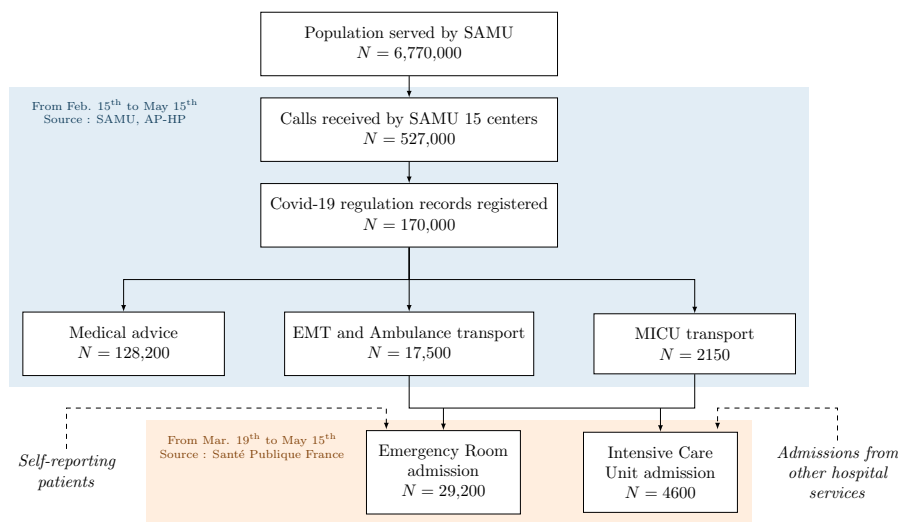


Figure 1: Flowchart: from calls to Center 15 to admission in hospital units. The numbers are summed over the departments 75, 92, 93 and 94 of the Paris area.

In order to maintain a rapid response when a major increase in the number of calls was observed, the four

Center-15 implemented specific procedures. Switchboard operators and medical staff was reinforced, and for calls related to Covid-19 an interactive voice server —triaging the calls to dedicated computer stations was developed. Patient evaluation and management were improved by introducing video consultation, sending of instruction using SMS, giving the patient the option to be called back. Prehospital EMT teams were also significantly reinforced by first aid volunteers, and additional MICU were created. Since January 20<sup>th</sup> 2020 all calls and patient records related to Covid-19 were flagged in the information system of Center-15 and a daily automated activity report was produced.

### 3 Methods

#### 3.1 Classification of calls

In order to develop a mathematical analysis of the evolution of the epidemic, we classified the calls tagged as Covid-19 in three categories, according to the decision taken:

Class 1: calls resulting in the dispatch of a Mobile Intensive Care Unit;

Class 2: calls resulting in the dispatch of an ambulance staffed with EMT;

Class 3: calls resulting in no dispatch decision. Such calls correspond to different forms of medical advice (recommendation to consult a GP, specific instructions to the patient, etc.).

We shall denote by  $Y_{\text{MICU}}(t)$  (resp.  $Y_{\text{EMT}}(t)$  and  $Y_{\text{adv}}(t)$ ) the number of MICU transports (resp. the number of ambulances transport and the number of medical advices) on day  $t$ , for patients tagged with suspicion of Covid-19. We shall call these functions of time the *observables*, in contrast with  $C(t)$ , the actual number of new contaminations on day  $t$ , which cannot be measured. We developed a piece of software that computes these observables by analyzing the medical decisions associated with the patient records, made accessible daily by AP-HP.

#### 3.2 Mathematical properties of the observables

To analyze the evolution of these observables, we rely on the SEIR-type mathematical models used to study the dynamics of Covid-19 [20, 9]. These are refinements of the original SEIR model, which has compartments representing susceptible, exposed and infected individuals, as well as individuals removed from the contamination chain. These refinements take into account the age structure of the population [20], or include additional compartments, representing, for instance, patients at hospital [9]. We shall assume that the population that has been infected is much smaller than the susceptible population. This approximation is reasonable at least in the initial part of the epidemic, according to the study [25] which gives an estimate of 5.7% for the proportion of the population in France that has been infected prior to May 11<sup>th</sup>, 2020. Then, the flow of the SEIR model becomes linear and order-preserving. The latter property entails that the observables are an increasing function of the initial population in the compartments of  $E, I$ -type. Results of Perron–Frobenius theory, which we recall in Section 7, entail that, *if the sanitary measures stay unchanged*, there is a rate  $\lambda$ , such that the number of newly contaminated individuals at day  $t$  grows as  $C(t) \simeq K_C \exp(\lambda t)$ , as  $t \rightarrow \infty$ , where  $K_C$  is a positive constant.

The number  $\delta := (\log 2)/\lambda$ , when it is positive, represents the *doubling time*: every  $\delta$  days, the number of new contaminations per day doubles. When  $\delta$  is negative, the epidemic is in a phase of exponential decay. Then, the opposite of  $\delta$  yields the time after which the number of new contamination per day is cut by half. For the analysis which follows, it is essential to consider, instead of  $C(t)$ , its logarithm,  $\log C(t) \simeq \log K_C + \lambda t$ . The exponential growth or decay of  $C(t)$  corresponds to a linear growth or decay of the logarithm.

It can also be shown that the observables grow or decay with the same rate. E.g., assuming that all the patients transported by MICU were contaminated  $\tau_{\text{MICU}}$  days before the transport, and that a proportion  $\pi_{\text{MICU}}$  of the contaminated individuals will require MICU transport, we arrive at  $Y_{\text{MICU}}(t) =$

$\pi_{\text{MICU}}C(t - \tau_{\text{MICU}})$ , and so  $\log Y_{\text{MICU}}(t) \simeq \log \pi_{\text{MICU}} + \log K_C + \lambda(t - \tau_{\text{MICU}})$ . Similar formulæ apply to  $Y_{\text{EMT}}$  and  $Y_{\text{adv}}$ . Therefore, *the logarithm of all the observables is asymptotically linear as  $t \rightarrow \infty$ , and the rate,  $\lambda$ , is independent of the observable.*

### 3.3 Piecewise linear approximation of the logarithm of the observables

When the sanitary measures change, for instance, when lockdown is established, the rate  $\lambda$  changes. So, the logarithm of the number of observables cannot be approximated any more by a linear function. However, a general result, stated as Theorem 1 below, shows that this logarithm can be approximated a *piecewise linear function* with as many linear pieces as there are phases of sanitary policy. This results stems from the order preserving and linear character of the epidemiological dynamics,

In the Paris area, there are three relevant sanitary phases to consider from February to May, 2020: initial growth (no restrictions); “stade 2” starting on Feb. 29<sup>th</sup> (prevention measures), and then lockdown from March 17<sup>th</sup> to May 11<sup>th</sup>. Sanitary phases are further described in Section 5.1.

Since the number  $\nu$  of sanitary phases is known (here  $\nu = 3$ ), we can infer the different values of  $\lambda$  attached to each of these phases, by computing the best piecewise linear approximation,  $\varphi(t)$  with at most  $\nu$  pieces of the logarithm of an observable  $Y(t)$ . To compute a robust approximation, we minimize the  $\ell_1$  norm,  $\sum_t |\varphi(t) - \log Y(t)|$ , where the sum is taken over the days  $t$  in which the data are available. Finding the best approximation  $\varphi$  is a difficult optimization problem, for the objective function is both non-smooth and non-convex. Methods to solve this problem are discussed in Appendix A.

### 3.4 Epidemic alarms based on doubling times

To construct epidemic alarms, we shall compute a linear fit,  $\varphi(t) = \alpha + \beta t$ , to the variables  $\log Y(t)$ , where  $Y$  is an epidemic observable. The principle is to trigger an alarm when the doubling time becomes positive, or equivalently, when the slope  $\beta$  becomes positive.

Assuming that values of  $Y(t)$  are known over a temporal window, there are simple ready-to-use methods for computing estimates  $\hat{\beta}$  for the slope  $\beta$ . We can also determine the probability  $p^+$  that the slope is positive. These methods are detailed in Section 9. On their basis, we propose the following **alarm raising mechanism, allowing one to deploy a gradual response**.

This mechanism relies on the two following observables,  $Y_{\text{adv}}$ , the number of calls resulting in medical advice, and  $Y_{\text{disp}} := Y_{\text{EMT}} + Y_{\text{MICU}}$ , the number of dispatched vehicles. The consolidation of the observables  $Y_{\text{EMT}}$  and  $Y_{\text{MICU}}$  is justified, because the two time series both correspond to the stage of aggravation, albeit with different degrees, and so they evolve more or less at the same time.

First define a temporal window of days  $t$  over which the linear fit  $\varphi_{\text{adv}}(t) = \alpha_{\text{adv}} + \beta_{\text{adv}}t$  to  $\log Y_{\text{adv}}(t)$  is made. By default we consider the last ten days prior to the current day. Similarly, we compute a linear fit  $\varphi_{\text{disp}}(t) = \alpha_{\text{disp}} + \beta_{\text{disp}}t$  to  $\log Y_{\text{disp}}(t)$  over the same time window.

Our algorithm will generate both a *warning* and *alarms*. A warning is a mere incentive to be careful. An unjustified warning is bothersome but generally harmless, so we accept a high probability of false positive for warnings. An alarm may imply some actions, so we wish to avoid false alarms. For this reason, we shall consider two different probability thresholds,  $\vartheta_{\text{alarm}}$  and  $\vartheta_{\text{warn}}$ , say  $\vartheta_{\text{alarm}} = 75\%$  and  $\vartheta_{\text{warn}} = 25\%$ . With this setting, we will be warned as soon as the probability of the undesirable event is  $\geq 25\%$ , and we will be alarmed when the same probability becomes  $\geq 75\%$ . Of course, these thresholds can be changed, depending on the risk level deemed to be acceptable. We shall denote by  $p_{\text{adv}}^+$  the probability that the slope  $\beta_{\text{adv}}$  is positive, and by  $p_{\text{disp}}^+$  the probability that  $\beta_{\text{disp}}$  is positive. These probabilities are evaluated on the basis of statistical assumptions detailed in Section 9.

1. A **warning** is provided when  $p_{\text{adv}}^+ \geq \vartheta_{\text{warn}}$ , meaning that the probability that the slope  $\beta_{\text{adv}}$  of the curve of the logarithm of the *calls for medical advice* over the corresponding time window be positive is at least  $\vartheta_{\text{warn}}$ . This should be interpreted as a mere warning of epidemic risk: choosing  $\vartheta_{\text{warn}}$  as above, the odds are at least 25% that the epidemic is growing.

2. This warning is subsequently transformed into an **alarm** when  $p_{\text{adv}}^+ \geq \vartheta_{\text{alarm}}$ . Choosing  $\vartheta_{\text{alarm}}$  as above, the odds that the epidemic is growing is now at least 75%.
3. Such an alarm is then subsequently transformed into a **confirmed alarm** if we still have  $p_{\text{adv}}^+ \geq \vartheta_{\text{alarm}}$ , and if, in addition,  $p_{\text{disp}}^+ \geq \vartheta_{\text{alarm}}$ , meaning that the probability that the slope of the logarithm of the curve of ambulances and MICU dispatches be positive is now above  $\vartheta_{\text{alarm}}$ . Again, this estimate is defined in terms of a time window over which  $\beta_{\text{disp}}$  is estimated. We use the same default values of ten days and  $\vartheta_{\text{alarm}}$  as above.

As shown in Section 4, the indicators based on vehicle dispatch are by far less noisy than the indicators based on calls for medical advices, but their evolution is delayed. This is the rationale for using medical advice for an early warning and early alarm, and then vehicle dispatch for confirmation.

Instead of considering the probability  $p^+$ , we could consider the upper and lower bounds of a confidence interval  $[\beta_\epsilon^-, \beta_\epsilon^+]$  for the estimated slope  $\beta$ , with a probability threshold  $\epsilon$ . Then we may, trigger a warning when  $\beta_\epsilon^+ \geq 0$ , and an alarm when  $\beta_\epsilon^- \geq 0$ . This leads to an essentially equivalent mechanism. We prefer the algorithm above as it allows to interpret the thresholds in terms of false positives and false negatives.

Given the severity of the risk implied by Covid-19, it is desirable to complete the previous alarm, based only on tail probabilities of the slope, by a different type of alarm, based on a threshold of doubling time,  $D$ . The alarm will be triggered if the odds that the doubling time be positive and smaller than  $D$  are at least one half. An indicative value of  $D$  might be 14 days: a doubling of the number of arrivals of Covid-19 patients in hospital services every 14 days may be quite challenging, justifying an alarm, and the slope corresponding to this doubling time seems significant enough to avoid false alarms. Again, the value of  $D$  can be changed arbitrarily depending on the acceptable level of risk. Moreover, this other type of alarm can still be implemented in two stages: early alarm, with the medical advice signal, and then confirmed alarm, with the vehicle dispatch signal.

In addition, Section 9 provides more sophisticated ready-to-use methods for obtaining sharper confidence intervals or probabilities for the slope  $\beta$ , resulting in more precise alarm mechanisms, when different time series are available. We require, however, that these series correspond to events occurring approximately at the same stage in the pathology unfolding. Here, we used the trivial aggregator,  $Y_{\text{disp}} = Y_{\text{EMT}} + Y_{\text{MICU}}$ . There is an optimal way to mix different series to minimize the variance of the composite estimator, explained in Section 9.

This methodology is generic. It could thus also apply to obtain a sharper confidence interval for the early indicator by combining its estimate  $\hat{\beta}_{\text{adv}}$  with that of other time series associated with signals that correspond to the same stage in pathology unfolding. Specifically, the count  $Y_{\text{GP}}(t)$  of patients consulting general practitioners for recently developed Covid-19 symptoms, if available, provides such a signal. A linear fit to  $\log Y_{\text{GP}}(t)$  would then yield an estimate  $\hat{\beta}_{\text{GP}}$  which can be combined with  $\hat{\beta}_{\text{adv}}$  to refine the corresponding confidence interval. In this way, we can mix several early but noisy indicators to get an early but less noisy consolidated indicator.

## 4 Results – data analysis

### 4.1 Key figures and graphs

From February 15<sup>th</sup> to May 15<sup>th</sup>, we counted a total of 170,166 patient files tagged with a suspicion of Covid-19, distributed as follows in the different departments: 53,646 in Dep. 75; 36,721 in Dep. 92; 49,703 in Dep. 93; and 30,096 in Dep. 94.

The flow of calls to the SAMU of the Paris area, and its impact on ER and ICU, is shown on Figure 1. The data concerning the ER and the ICU are taken from the governmental website SPF (Santé Publique France) [10], it is available only from March 19<sup>th</sup>.

On Figure 2, we represent, in logarithmic ordinates, the numbers of events of different types, summed over the four departments of the Paris area (75, 92, 93 and 94): (i) the number of patients calling the SAMU (including patients not calling for Covid-19 suspicion); (ii) the number of calls tagged as Covid-19

not resulting in a vehicle dispatch (i.e., as discussed in §3.1, all kinds of medical advices); (iii) the number of calls tagged as Covid-19 resulting in an ambulance or MICU dispatch,

We obtained the data (i) by analyzing the phone operator log files. Since a patient may call the Center 15 several times, we eliminated multiple calls to count unique patients. To compute data (ii) and (iii), we developed a software to analyze the “medical decision” field of the regulation records.

Using logarithmic ordinates is essential on Figure 2, as it allows to visualize on the same graph signals of different orders of magnitude (e.g, there is a ratio of 20 between the peak number of patients calling and the peak number of vehicles dispatched).

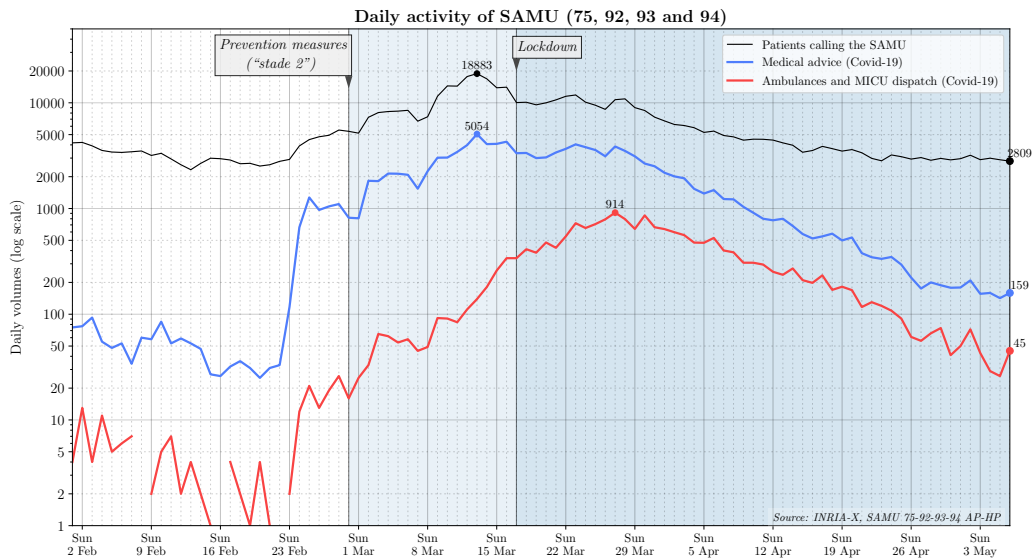


Figure 2: Number of patients calling Center-15, of MICU and ambulances dispatch for Covid-19 suspicion in the Paris area (departments 75, 92, 93 and 94)

The evolution of the number of vehicles dispatched (MICU and ambulances) is shown on Figure 3, for each department of the Paris area (still with logarithmic ordinates).

We provide in Table 1 the doubling times of the number of vehicles dispatched (ambulances and MICU), for the different departments, measured in days (abbreviation “d”).

	Feb. 28 <sup>th</sup> – Mar. 15 <sup>th</sup>	Mar. 15 <sup>th</sup> – Mar. 29 <sup>th</sup>	Mar. 29 <sup>th</sup> – April 24 <sup>th</sup>
75	5.9 d	9.8 d	-9.4 d
92	4.9 d	10.6 d	-8.3 d
93	4.2 d	8.5 d	-10.2 d
94	4.6 d	6.9 d	-7.7 d

Table 1: Doubling time of the number of MICU and ambulances dispatched, for different periods, for each department, obtained by a least squares approximation of the logarithm of this number. The opposite of a negative doubling time yields the halving time.

We now draw several conclusions from the previous analysis.

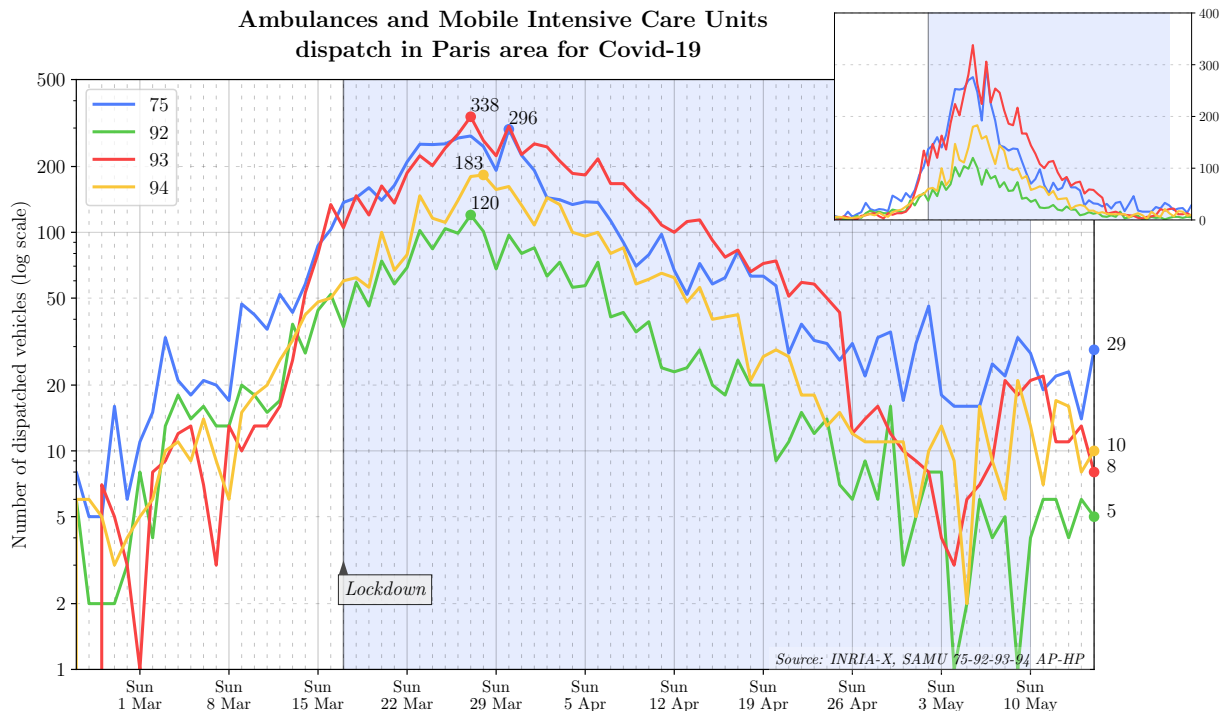
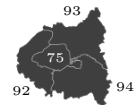


Figure 3: Comparison of the evolution of the epidemic in the different departments of the Paris area: numbers of vehicles dispatch by department. The figure inset displays the same curves in usual linear ordinates to keep in mind the different magnitudes at stake. A map of the Paris area, showing the departments 75, 92, 93, 94, is at the bottom right of the figure.





## 4.2 The increase in the number of calls for medical advice provides an early, but noisy, indicator of the epidemic growth

As shown in Figure 2, the peak of the number of calls for medical advice was on March 13<sup>th</sup>. However, this date, four days before the lockdown (March 17<sup>th</sup>), is not consistent with epidemiological modeling. This peak seems rather to be caused by announcements to the population, see the discussion in Section 6.1.

## 4.3 The epidemic kinetics vary strongly across neighboring departments

In the initial phase of the epidemic (Feb. 28<sup>th</sup>–March 15<sup>th</sup>), the doubling time was significantly shorter in the 93 department (4.2 d) than in central Paris (5.9 d). The 93 department, with 1.6M inhabitants, is less populated than central Paris (2.1M inhabitants). Another difference between the departments concerns mobility. Movement from the population from central Paris to smaller towns and cities or to countryside were observed, after March 12<sup>th</sup>, the date of the first presidential address concerning the Covid-19 crisis.

In order to quantify this mobility, we requested information from Enedis, the company in charge of the electricity distribution network in France, and also from Orange and SFR, two operators of mobile phone networks.

Enedis provided us with an estimation of the departure rates of households, based on a variation of the volume of electricity consumed, aggregated at the level of departments and districts (i.e., *arrondissements*).

SFR provided us with estimates of daily flows from the Paris area to other regions, again aggregated at the scale of the departments or districts, based on mobile phone activity, confirming this decrease of population.

Orange Flux Vision provided us with daily population estimates, at the scale of department, based on mobile phone activity. By March 30<sup>th</sup>, the population, during the night, was estimated to be 1.6M inhabitants in central Paris, versus 1.35M in the 93.

However, the epidemic peak was higher in the 93 than in the 75 (338 dispatches versus 296). The contraction rate in the period after the peak (March 29<sup>th</sup>–Apr. 24<sup>th</sup>) was also smaller in the 93, with a halving time of 10.2 days, to be compared with 9.4 days in the 75. Possible explanations for these strong spatial discrepancies are discussed in Section 6.5.

# 5 Results – mathematical modeling

## 5.1 Delay between implementation of sanitary policies and its effect on hospital admissions

The best approximation, in the  $\ell_1$  norm, of the logarithm of the number of vehicles dispatched (ambulances and MICU), by a piecewise linear map with at most three pieces, is shown on Figure 4. This is done with the method of Appendix A.

In order to evaluate the influence of a sanitary measure on the growth of the epidemic, an approach is to compare the date of the measure with the date of the change of slope of the logarithmic curve, consecutive to the measure. This method is expected to be more robust than, for instance, a comparison of peak values, because the best piecewise-linear approximation is obtained by an optimization procedure *taking the whole sequence into account*. Indeed, a local corruption of data will not change significantly the date of change of slope, if the problem is *well conditioned*. This is the case in particular if the difference between consecutive slopes is sufficiently important. In other words, we can identify in a more robust manner the time of effect of a strong measure than of a mild one.

Let us recall the main changes of sanitary measures in the Paris area, between February and May 2020. We may distinguish the following phases:

- *Initial development of the epidemic*, no general sanitary measures in the Paris area, until Feb 29<sup>th</sup>, first day of so-called “stade 2” by the authorities (following “stade 1” in which measures intended to prevent the introduction of the virus in France – like quarantine in specific cases– were taken).

- “*Stade 2*” (*stage 2*) *measures*: general instructions of social distancing given to the population (e.g., not shaking hands), ban on large gatherings. Moreover, some large companies created crisis committees, and decided to take more restrictive measures than the ones required by the authorities, including for instance banning meetings with more of 10 people, and banning business travels. Restrictive measures in companies were deployed gradually during the work week from March 2<sup>nd</sup> to March 6<sup>th</sup>.
- *School closure* on March 16<sup>th</sup>.
- *Lockdown* on March 17<sup>th</sup>. The lockdown ended on May 11<sup>th</sup>, throughout the country.

Hence, we may interpret the variations in the slope in the piecewise linear approximation of the logarithm of the number of ambulances and MICU dispatched, shown on Figure 4, as the effect of sanitary measures. The dates where the slope changes are represented in the figure by dotted lines. Thus, the latest breakpoint of the piecewise linear approximation of the 75 curve (in blue) arises on March 26<sup>th</sup>, to be compared with March 30<sup>th</sup> in the 93 (red curve). The dates of breakpoints in the 92 and 94 are intermediate. Given the first strong measure (closing of schools) was taken on March 16<sup>th</sup>, we may evaluate the delay between a sanitary measure and its effect on the ambulances and MICU dispatch to be between 10 and 14 days. This corresponds to a delay between contamination and occurrence of severe symptoms.

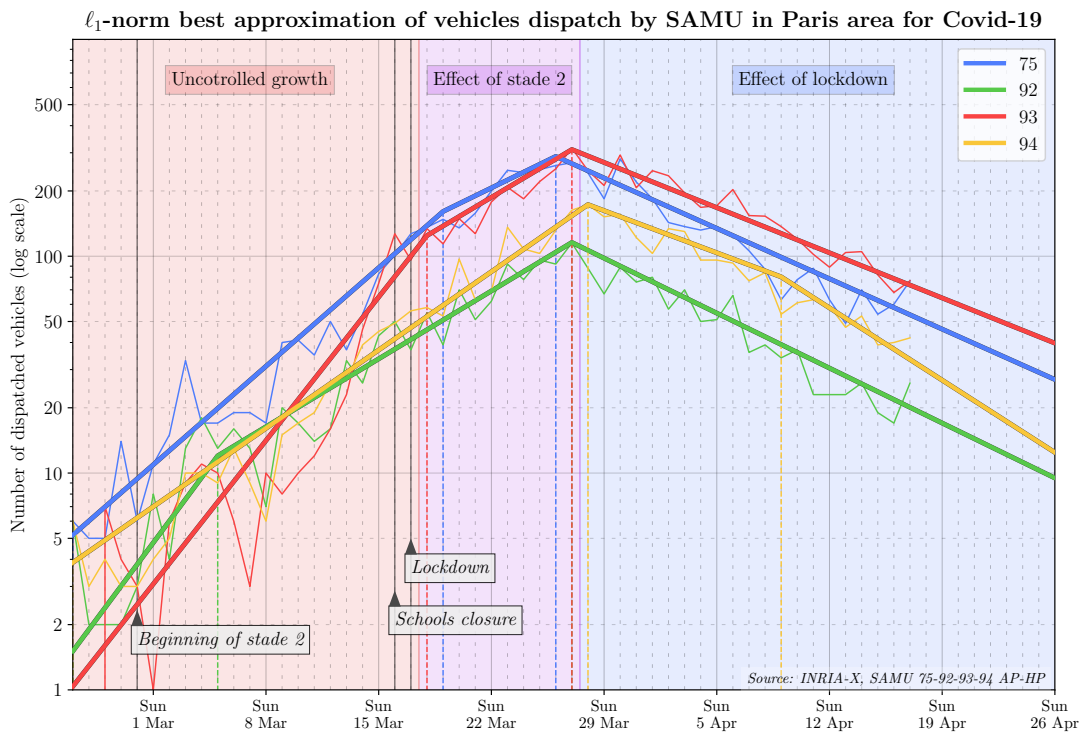


Figure 4: Logarithm of the number of ambulances dispatched: the effect of the successive sanitary measures

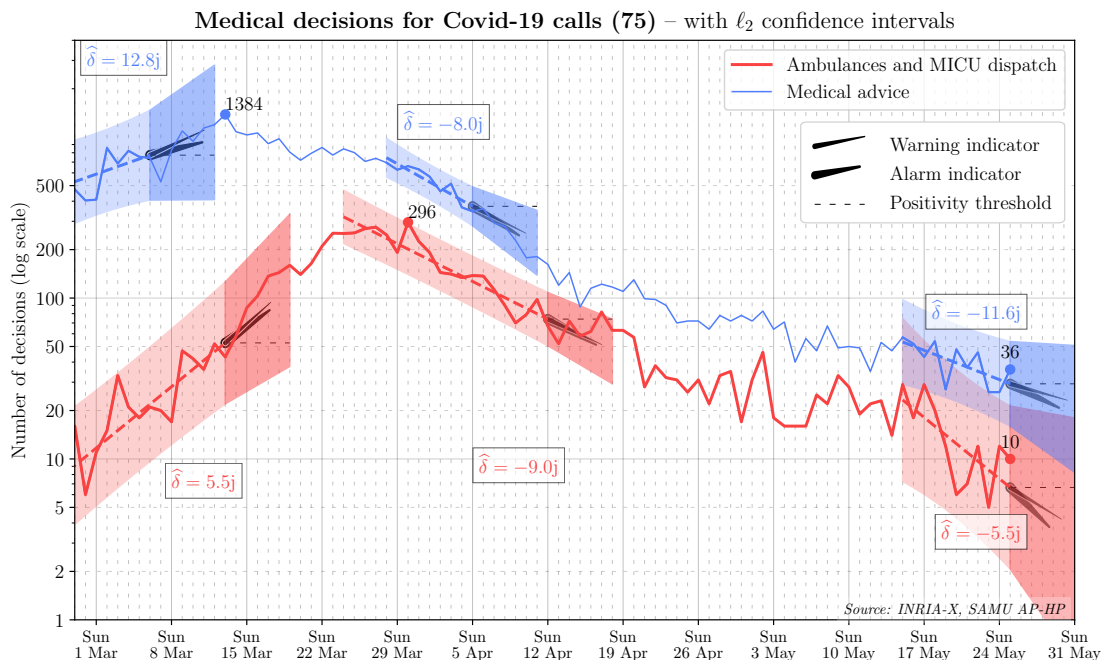


Figure 5: Short term predictor for SAMU 75, with confidence regions and warning and alarms indicators

## 5.2 Construction of statistical indicators of epidemic resurgence based on emergency calls

We implemented the alarm mechanism based on the inference of doubling times described in Section 3.4 and further explained in Section 9. The method is illustrated on Figure 5. Given a time period where the data is known, we perform a linear regression on the number of medical advices and vehicles dispatched.

The light shaded, tubular areas around the curves are based on confidence intervals for the fluctuations of the observed log-counts. The dark-shaded, trapezoidal areas prolongate the tubular areas with straight lines, the slopes of which correspond to confidence intervals for the slope of the linear regression. We display such confidence domains for the last known data in May, performing a 6-day forecast based on the last ten days. In order to validate the method, we also display these domains for older data in March and April, performing for each a 6-day forecast based on a number of past days. For these time-periods, the short-term confidence domains are seen to satisfactorily contain the data of the following days. Observe how the shape of the confidence trapezoids depends on the number of points and the variance of the data used to compute them.

The needle-shaped (or clock hand) indicators depicted in each trapezoidal confidence domain illustrate the alarm mechanism of Section 3.4. For each slope inference, there is a  $\vartheta_{\text{warn}} = 25\%$  probability that the real-value of the slope we estimated using recent data is greater than the slope of the thin needle on the picture. Likewise there is a  $\vartheta_{\text{alarm}} = 75\%$  probability that the real slope is greater than the slope of the fat hand. As a result, a warning (resp. an alarm) on the dynamics of the medical advice curve should be triggered as soon as the thin needle (resp. the fat needle) has a positive angle with respect to the horizontal. We have depicted the horizontal with dashed lines to enhance readability.

On May 22<sup>nd</sup>, the warning is triggered, since the probability that the slope of the logarithm of the blue curve is positive is  $> 25\%$ . However, the estimated slope is negative, although marginally so, with a halving time of 52.1 days, and the probability that the slope is positive is  $< 75\%$ , so no alarm is triggered. A fortiori,

no alarm confirmation is triggered either.

The numbers  $\vartheta_{\text{warn}}$  and  $\vartheta_{\text{alarm}}$  need to be carefully calibrated, and for this, additional data for the forthcoming weeks may be helpful.

## 6 Discussion

### 6.1 Calls resulting in medical advice are highly influenced by the instructions given to the population

The blue curve on Figures 2 and 5 counts the number of times medical advices was given, of all kinds (calls resulting in recommendations given to the patient but no vehicle dispatched). It is generally associated with early events in the unfolding of the pathology, and in particular occurrence of the first symptoms. An estimate of 5.2 days between the date of contamination and the date of the first symptoms is given in [18], so we may assume that calls for medical advice are made by patients 5-8 days after contamination. We observed in Section 4.2 that the peak in the number of calls resulting in medical advice was on March 13<sup>th</sup>. Hence, assuming a regime of epidemic growth before lockdown, the peak of the curve of new symptom occurrences must occur *only several days after the lockdown time* (March 17<sup>th</sup>). This indicates that the curve of calls resulting in a medical advice did not give a reliable picture of the epidemic growth around March 13<sup>th</sup>. Indeed, this curve is very sensitive to changes in the instructions given to the population and to political announcements, notable examples of which include the following: recommendation to patients to call emergency number 15, instead of going directly to emergency departments (to avoid contamination and overcrowding); – the presidential announcement on March 12<sup>th</sup> of more restrictive measures to be deployed from March 16<sup>th</sup>, making the population more aware of the growth of the epidemic.

### 6.2 The indicators of medical advice given and ambulances and MICU dispatch can be used to monitor the epidemics

Setting aside perturbations due to political announcements or changes in the policy for calling SAMU, the curve of calls for medical advice should be a reliable and early estimate of the curve of ambulances dispatched, which is triggered at a later stage in the unfolding of the pathology when symptom severity increases. Thus, it gives an early signal allowing both SAMU and hospitals to anticipate by several days an increase in load.

We can give a rough estimate of this delay by considering the peak dates in Figure 2. Epidemiological modeling indicates that the number of new contaminations grows exponentially until a sanitary measure that is strong enough to contain the epidemic is taken. In the present case, the candidates for such strong measures are the school closing (March 16<sup>th</sup>) or the lockdown (March 17<sup>th</sup>). Considering the last day previous to the measures, we may assume that the peak date for new contaminations was on March 15<sup>th</sup> or March 16<sup>th</sup>. As mentioned above, according to [18], the time between contamination and first symptoms is estimated to be 5.2 days. Hence, if calls for medical advice were representative of first symptoms, the peak value for these calls would have been between around March 20<sup>th</sup> or March 21<sup>st</sup>. The peak of the number of dispatches of ambulances and MICU was on March 27<sup>th</sup>. This leads to an estimate of 6-7 days for the delay between the curve of the true need for medical advice and the curve of vehicles dispatch.

The alarm mechanism was developed during the crisis, after March 20<sup>th</sup>. Had it been available before, in the 75, the early warning would have occurred by February 24<sup>th</sup> (for both Covid-19 indicators on medical advice and vehicle dispatch), alarm would have been triggered on February 25<sup>th</sup> based on medical advice, and a confirmation alarm would have occurred on February 27<sup>th</sup> based on ambulance and MICU dispatch.

Tracking the same signal at a finer spatial resolution (a neighborhood rather than a department) may enable epidemic surveillance during the period following the lifting of measures such as travel bans. Indeed in view of the spatial differentiation in doubling times at the department level, it appears plausible that disparities may also be present at much finer spatial granularities, with resurgences localized to towns or

neighborhoods. Deployment of alarm mechanisms constructed from event counts at finer spatial granularities could be used to identify clusters of resurgence early on, and guide subsequent action.

Seasonal influenza, whose early symptoms can be mistaken for those of Covid-19, can also trigger a linear growth of the logarithms of the number of calls, or vehicle dispatched. However the slope of this logarithmic curve is expected to be shallower, owing to the lower contagiousity of influenza. One could thus distinguish, on the basis of the observed slope, whether one is confronted with seasonal flu or with an outbreak of Covid-19.

### **6.3 Jumps of the curves of the number of calls may be caused by large clusters or influenced by neighboring countries**

The curves of the number of calls for medical advice, and of vehicles dispatched (Figure 2), both jump between February 23<sup>rd</sup> and 25<sup>th</sup>. Epidemiological models are unlikely to produce shocks of this type in the absence of exceptional factors. Several significant epidemic events occurred at nearby dates, including:

1. The development of the Covid-19 epidemic in the north of Italy, a region closely tied to France (the first lockdowns occurred around February 21<sup>st</sup> in the province of Lodi). The school vacation ended on February 23<sup>th</sup> in the Paris area. A significant number of Parisians went back from Italy during the week-end of February 22<sup>nd</sup>-23<sup>th</sup> (end of school vacation).
2. A large Evangelist meeting (Semaine de Carême de l’Eglise La Porte Ouverte Chrétienne de Bourzwiller, Haut-Rhin), from February 17<sup>th</sup> to February 21<sup>st</sup>, identified by Agence Régionale de Santé Grand Est as the source of a cluster phenomenon [8].

The potential influence of the north Italy epidemic was pointed out by Paul-Georges Reuter (private communication). At this stage, the essential factors are not yet known. The influence of mobility on the development of the epidemic in the Paris area will be studied in a further work.

### **6.4 Patients from different areas tend to call the SAMU at different stages of the pathology**

Considering the piecewise linear curves in Figure 4, we note that in the 93, the date of the break point is shifted of 3 days, by comparison with the 75, suggesting that by this time, the patients of 93 were calling Center 15 at a later stage of the evolution of the disease. This hypothesis is confirmed by an examination of the ratio of the number of MICU dispatched over the number of ambulances dispatched. For instance, on March 30<sup>th</sup>, there were 9 MICU dispatches and 276 other dispatches in the 75, to be compared with 25 MICU dispatches and 262 other dispatches in the 93, i.e., ratios of 3.3% in the 75 and 9.5% in the 93.

In the same way, the first breakpoints of the curves give an indication of the times at which “stade 2” measures influence the epidemic growth. These dates range from March 15<sup>th</sup> (for 92) to March 22<sup>nd</sup> (for 75). It may be the case that these dates are dispersed because the change of slope is relatively small, meaning that the effect of stade 2 is mild. Indeed, the milder the slope change, the more the estimation of the corresponding date is sensitive to noise. Another effect which may have perturbed the curves is the important mobility of the population in the 4 departments, between March 12<sup>th</sup> and March 16<sup>th</sup>.

### **6.5 The strong spatial heterogeneity of the evolution of the epidemic may be explained by local conditions**

We observed in Section 4.3 that in the initial phase of the epidemic (Feb. 28<sup>th</sup>–March 15<sup>th</sup>), the doubling time was significantly shorter in the 93 department, whereas in the contraction phase, the halving time was significantly higher.

One may speculate that the contraction rate in the lockdown phase is influenced by intra-familial contaminations. In this respect, according to a survey of INSEE, the national institute of statistics, the average size of a household is of 2.6 in the 93, versus 1.9 in the 75 (values in 2016 [13]).

We also remark that just after the peak on March 27, and up to April 6, the curve of the department 93 on Figure 3 has the shape of a high, oscillating plateau, decaying more slowly than the curve of the department 75. This may be caused by changes in the nature of the dominant mode of contaminations, intra-familial contamination becoming an essential part of the kinetics during lockdown.

One may also speculate that the blowup rate in the initial phase is higher when the population is more dependent on public transport, or working in jobs with more contamination risk. These aspects will be further studied elsewhere.

After Stade 2 was announced, during the period from March 2<sup>nd</sup> to March 6<sup>th</sup>, a number of large companies took specific measures (e.g., forbidding avoidable small group meetings, enforcing travel restrictions, restricting office access), in addition to the general measures (not shaking hands, forbidding large meetings) enforced by the authorities. This may have led to a decrease of the number of contamination on the workplace, and one explanation for the increase of the doubling time.

## 7 Epidemiological model based on transport PDE

We now present mathematical models that can be used to represent the dynamics of the Covid-19 epidemic.

We introduce a multi-compartment transport PDE model. This model has the same type of compartments as the usual SEIR ODE models. SEIR ODE models assume that the transition time from a compartment to the next one has an exponential distribution. This implies, in particular, that an exposed individual can immediately become infectious. In contrast, transport PDE models allow us to capture the situation in which the transition times are bounded away from 0. This is an essential feature in the case of Covid-19, since, according to [18], the transition time from the exposed state to the infectious state is estimated to a minimum of 2 days, with a median of 5.2 days.

Recall that the basic SEIR model consists of four compartments, namely: (S) for susceptible, (E) for exposed (those individuals infected although not yet infectious), (I) for infectious and finally (R) for removed (no longer infectious, whether deceased or immunized). The number of individuals within each compartment then evolves according to an Ordinary Differential Equation given e.g. in [1]. This SEIR model can be enriched by introducing additional compartments detailing for instance age ranges, distinct types of symptoms (asymptomatic or symptomatic, with various levels of severity), admission to distinct hospital services (see e.g. [20] and [9]).

We shall keep the same compartments  $S, E, I, R$ , but the state variables attached to the  $E$  and  $I$  compartments will take the time elapsed in the compartment into account, and thus, will be infinite dimensional.

For all  $t \geq 0$ , we denote by  $n_E(x, t)$  the density of the number of individuals that were contaminated  $x$  time units before time  $t$ , and that are not yet infectious at time  $t$ , i.e., the number of exposed individuals that began to be exposed at time  $t - x$ . Then, the size of the exposed population at time  $t$  is given by

$$E(t) = \int_0^\infty n_E(x, t) dx . \quad (1)$$

Similarly, we denote by  $n_I(x, t)$  the density of the number of individuals that became infectious  $x$  time units before time  $t$ , and that are not yet removed from the contamination chain at that time. Then, the size of the infectious population at time  $t$  is given by

$$I(t) = \int_0^\infty n_I(x, t) dx . \quad (2)$$

Finally, we denote by  $S(t)$  the number of susceptible individuals at time  $t$ , and by  $R(t)$  the number of individuals that have been removed from the contamination chain before time  $t$ .

The total population at time  $t$  is given by

$$N(t) := S(t) + E(t) + I(t) + R(t) .$$

We consider the following system of PDE and ODE, with integral terms in the boundary conditions:

$$\frac{dS}{dt} = -\frac{S(t)}{N(t)} \int_0^\infty K_{I \rightarrow E}(x, t) n_I(x, t) dx , \quad (3a)$$

$$n_E(0, t) = \frac{S(t)}{N(t)} \int_0^\infty K_{I \rightarrow E}(x, t) n_I(x, t) dx , \quad \frac{\partial n_E}{\partial t}(x, t) + \frac{\partial n_E}{\partial x}(x, t) + K_{E \rightarrow I}(x, t) n_E(x, t) = 0 , \quad (3b)$$

$$n_I(0, t) = \int_0^\infty K_{E \rightarrow I}(x, t) n_E(x, t) dx , \quad \frac{\partial n_I}{\partial t}(x, t) + \frac{\partial n_I}{\partial x}(x, t) + K_{I \rightarrow R}(x, t) n_I(x, t) = 0 , \quad (3c)$$

$$\frac{dR}{dt} = \int_0^\infty K_{I \rightarrow R}(x, t) n_I(x, t) dx . \quad (3d)$$

We assume an initial condition at time 0,  $S(0)$ ,  $n_E(\cdot, 0)$ ,  $n_I(\cdot, 0)$  and  $R(0)$  is given.

This model is inspired by the so called ‘‘age structured models’’ considered in population dynamics [24, 21], and used in particular to model the cell cycle. Here, ‘‘age’’ refers to the age in a compartment, it should not be confused with the age (time elapsed since birth) considered in epidemiological models.

We suppose that  $K_{I \rightarrow E}$ ,  $K_{E \rightarrow I}$  and  $K_{I \rightarrow R}$  are given *nonnegative* functions. The value  $K_{E \rightarrow I}(x, t)$  gives the departure rate from the compartment  $E$  to the compartment  $I$ , for individuals of ‘‘age’’  $x$  in the compartment  $E$ , at time  $t$ . Similarly,  $K_{I \rightarrow R}(x, t)$  gives the departure rate from the compartment  $I$  to the compartment  $R$ . As in the classical SEIR model, the departure term from the susceptible compartment, i.e., the right-hand-side of (3a) is bilinear in the number  $S(t)$  of susceptible individuals and in the population of infectious individuals  $n_I(\cdot, t)$ , and we normalize by the size of the population  $N(t)$ . The term  $K_{I \rightarrow E}(x, t)$  can be interpreted as an infection rate. We shall assume that this rate has the product form

$$K_{I \rightarrow E}(x, t) = \alpha(t) \psi(x) .$$

Thus, the infectiosity of an individual depends on his ‘‘age’’ in the infectious phase. The term  $\alpha(t)$  represents the control of the epidemia by sanitary measures (social distancing, wearing masks, closing schools, lockdown, etc.). We shall assume that the infectiosity rate  $K_{I \rightarrow E}(x, t)$  is the only parameter which can be controlled, hence,  $\alpha(\cdot)$  is a decision variable, whereas the function  $\psi(\cdot)$  is fixed. Moreover,  $K_{E \rightarrow I}(x, t) = K_{E \rightarrow I}(x)$  and  $K_{I \rightarrow R}(x, t) = K_{I \rightarrow R}(x)$  will be given functions, independent of time.

Differentiating  $N(t)$  with respect to time, using the system above, and assuming that for all  $t \geq 0$ ,  $n_E(x, t)$  and  $n_I(x, t)$  vanish when  $x$  tends to infinity, we verify that the total population  $N(t)$  is independent of time.

When the functions  $K_{I \rightarrow E}$ ,  $K_{E \rightarrow I}$  and  $K_{I \rightarrow R}$  are constant, taking into account (1) and (2), we recover the classical SEIR model from the dynamics (3):

$$\dot{S} = -\frac{S}{N} K_{I \rightarrow E} I , \quad (4a)$$

$$\dot{E} = \frac{S}{N} K_{I \rightarrow E} I - K_{E \rightarrow I} E , \quad (4b)$$

$$\dot{I} = K_{E \rightarrow I} E - K_{I \rightarrow R} I , \quad (4c)$$

$$\dot{R} = K_{I \rightarrow R} I . \quad (4d)$$

A variant of this model, in which  $K_{I \rightarrow E} = \alpha(t)$  depends on time (but not on  $x$ ) is considered in [5].

For epidemics in their early stages, i.e., when the number of individuals in the exposed, infectious, or removed compartments is negligible with respect to the number of susceptible individuals, the classical SEIR model is well-approximated by a linear system of Ordinary Differential Equations (see e.g. [1]) tracking only the populations in the (E) and (I) compartments. The study [25] estimates at about 5.7% the fraction of the French population exposed prior to May 11, which justifies reliance on this linear approximation in our context. The same approximation applies to the present PDE model. Hence, we suppose that  $S(t)/N(t) \simeq 1$ ,

and we are reduced to the following system:

$$n_E(0, t) = \int_0^\infty \alpha(t)\psi(x)n_I(x, t) dx , \quad \frac{\partial n_E}{\partial t}(x, t) + \frac{\partial n_E}{\partial x}(x, t) + K_{E \rightarrow I}(x)n_E(x, t) = 0 , \quad (5a)$$

$$n_I(0, t) = \int_0^\infty K_{E \rightarrow I}(x)n_E(x, t) dx , \quad \frac{\partial n_I}{\partial t}(x, t) + \frac{\partial n_I}{\partial x}(x, t) + K_{I \rightarrow R}(x)n_I(x, t) = 0 . \quad (5b)$$

This is a multi-compartment generalization of the renewal equation, studied in Chapter 3 of [24].

We associate to the PDE (5) a family of time evolution operators  $(T_{s,t})_{t \geq s \geq 0}$ , which maps an initial condition at time  $s \geq 0$ , that is a couple of functions  $n(\cdot, s) := (n_E(\cdot, s), n_I(\cdot, s))$ , to the couple of functions  $n(\cdot, t) := (n_E(\cdot, t), n_I(\cdot, t))$  at  $t \geq s$ . These operators are order preserving, meaning that, if  $n^1(\cdot, s)$  and  $n^2(\cdot, s)$  are two initial conditions such that  $n_E^1(x, s) \leq n_E^2(x, s)$  and  $n_I^1(x, s) \leq n_I^2(x, s)$  for all  $x \geq 0$ , then the inequalities  $n_E^1(x, t) \leq n_E^2(x, t)$  and  $n_I^1(x, t) \leq n_I^2(x, t)$  hold for all  $x \geq 0$  and for all  $t \geq s$ .

When the control  $\alpha(t)$  is constant and positive, the family of time evolution operators  $(T_{s,t})_{t \geq s \geq 0}$  is determined by the semigroup  $(S_t = T_{0,t})_{t \geq 0}$ , and the long term evolution of the dynamical system (3) can be studied by means of the Perron–Frobenius eigenproblem

$$\bar{n}_E(0) = \int_0^\infty \alpha\psi(x)\bar{n}_I(x) dx , \quad \frac{\partial \bar{n}_E}{\partial x}(x) + (\lambda + K_{E \rightarrow I}(x))\bar{n}_E(x) = 0 , \quad (6a)$$

$$\bar{n}_I(0) = \int_0^\infty K_{E \rightarrow I}(x)\bar{n}_E(x) dx , \quad \frac{\partial \bar{n}_I}{\partial x}(x) + (\lambda + K_{I \rightarrow R}(x))\bar{n}_I(x) = 0 , \quad (6b)$$

where  $\bar{n} := (\bar{n}_I(\cdot), \bar{n}_E(\cdot))$  is the eigenvector, and  $\lambda$  is the eigenvalue.

Systems of PDE of this nature have been studied in particular by Michel, Mischler and Perthame, see [21, 24], and also, with an abstract semigroup perspective, in the work by Mischler and Scher [22].

We make a simplifying technical assumption, which suffices to capture the epidemiological application.

**Assumption 1.** *The functions  $\psi(x)$  and  $K_{E \rightarrow I}(x)$  vanish for  $x > x_I^*$  and  $x > x_E^*$ , respectively, for some positive reals  $x_I^*$  and  $x_E^*$ .*

Then, the evolution of the PDE system (5) can be described only in terms of the restriction of the functions  $n_E(\cdot, t)$  and  $n_I(\cdot, t)$  to the intervals  $[0, x_E^*]$  and  $[0, x_I^*]$ , respectively. Working with a bounded interval allows us to apply results from Perron–Frobenius and Krein–Rutman theory. If the functions  $\psi(x)$ ,  $K_{E \rightarrow I}(x)$ , and  $K_{I \rightarrow R}(x)$  are measurable and bounded, the evolution of the couple  $n(\cdot, t) := (n_E(\cdot, t)|_{[0, x_E^*]}, n_I(\cdot, t)|_{[0, x_I^*]})$  of restricted functions is described by a family of linear evolution operators acting on the space  $L^1([0, x_E^*]) \times L^1([0, x_I^*])$ . Indeed, we can compute  $n(x, t)$  by the characteristics method provided we know either  $n(x-t, 0)$  when  $x \geq t$  or  $n(0, t-x)$  when  $t \geq x$ . The latter value can be obtained from  $n(\cdot, t-x)$  by using the initial conditions in (5).

We make another elementary assumption.

**Assumption 2.** *The functions  $\psi(x)$ ,  $K_{E \rightarrow I}(x)$ , and  $K_{I \rightarrow R}(x)$  are continuous on the intervals  $[0, x_I^*]$ ,  $[0, x_E^*]$  and  $[0, x_I^*]$ , respectively, and they are not identically zero.*

Then, compactness arguments allow us to establish the existence of a positive and continuous solution  $\bar{n} = (\bar{n}_E|_{[0, x_E^*]}, \bar{n}_I|_{[0, x_I^*]})$ , of the (restricted) eigenproblem (6). Our assumptions may be relaxed. However, we need to assume that the functions  $\psi(x)$ ,  $K_{E \rightarrow I}(x)$ , and  $K_{I \rightarrow R}(x)$  do not vanish on some sets of non-zero measures, to guarantee the irreducibility of the semigroup. We refer the reader to [21, 22] for more advanced results, using less demanding assumptions. We also point out that the relative entropy inequality technique of [21] allows one to establish the convergence of  $n(\cdot, t)$  to the eigenvector, modulo multiplicative constants, as  $t$  tends to infinity.

A fortiori, the previous analysis applies to finite dimensional models. Instead of the transport PDE (5), we consider an ODE of the form

$$\dot{v} = Mv \quad (7)$$



where  $v(t) \in \mathbb{R}^n$  and  $M$  is a  $n \times n$  matrix with non-negative off-diagonal terms, a so-called *Metzler matrix*. In the original SEIR model [1], the matrix  $M$ , obtained by considering the  $(E, I)$ -block equations (4b), (4c), with  $S/N \simeq 1$ , is of dimension 2. In the generalizations of the SEIR model considered in [20, 9], the dimension  $n$  is increased to account for other compartments. One can also discretize the PDE system (5) using a monotone (upwind) finite difference scheme, and this leads to a system of the form (7).

In all these finite dimensional models, the matrix  $M$  is Metzler and irreducible. Then, the Perron–Frobenius theorem for linear, order-perserving semigroups (see [3]) implies that  $M$  admits a unique eigenvalue  $\lambda$  of maximal real part. Furthermore  $\lambda$  is algebraically simple and real, and its associated eigenvector  $u$  has strictly positive coordinates. Then, it follows from the spectral theorem that

$$v(t) = \exp(\lambda t)u + o(\exp(\lambda t))$$

as  $t \rightarrow \infty$ .

In all these models, any epidemic observable, for instance, the number of ambulances that are dispatched, can be obtained by applying a continuous linear form to the state variable. This state variable is  $n(\cdot, t) = (n_E(\cdot, t), n_I(\cdot, t))$  in the PDE case, or  $v(t)$  in the discrete space case. Moreover, this linear form takes nonnegative values on nonnegative functions, or vectors.

For instance, we may assume that the number of dispatches of ambulances at time  $t$  is given by the expression

$$Y_{\text{disp}}(t) = \int_{\underline{x}}^{\bar{x}} \kappa(x) n_I(x, t) dx ,$$

where  $\kappa(x)$  is a nonnegative continuous function, and  $\underline{x}$  and  $\bar{x}$  are lower and upper bounds for the “ages” in the compartment  $I$  at which aggravation may arise.

## 8 Tropicalization of the logarithm of nonnegative observables of switched Perron–Frobenius dynamics

We introduce an abstract setting, which captures epidemiological models in which most individuals are susceptible. This setting applies, in particular, to the transport PDE model of (5), when the transition functions are supported by compact intervals, and to the general finite dimensional Metzler model (7).

We consider  $(V, \leq)$ , a partially ordered Banach space, with topological dual  $V'$ . We denote by  $V_{\geq 0} := \{v \in V \mid v \geq 0\}$  the set of nonnegative elements of  $V$ , which is a convex cone. This cone must be pointed (i.e.,  $V_{\geq 0} \cap (-V_{\geq 0}) = \{0\}$ ), since the relation  $\leq$  is a partial order. We require this cone to be closed.

We consider a sequence of  $m$  semigroups  $S^i = (S^i_t)_{t \geq 0}$ , for  $i \in [m]$ , where  $[m] := \{1, \dots, m\}$ . We assume that for all  $i \in [m]$ , and for all  $t \geq 0$ ,  $S^i_t$  is a bounded linear operator from  $V$  to itself, and that the semigroup property holds, i.e.,  $S^i_{t+s} = S^i_t \circ S^i_s$ . We shall say that the semigroup  $S^i$  is *order preserving* if, for all  $v \in V_{\geq 0}$ , and for all  $t \geq 0$ ,  $S^i_t v \in V_{\geq 0}$ .

We shall consider commutation instants,  $t_0 := 0 < t_1 < \dots < t_{m-1}$ . These instants will correspond to significant epidemiological dates, for instance, dates at which sanitary measures are taken. We set  $t_m := +\infty$ .

We select an initial condition  $v_0 \in V_{\geq 0}$ , and consider the abstract dynamical system obtained by switching between the evolutions determined by the semigroups  $S^1, \dots, S^m$ , at the successive times  $t_1, \dots, t_{m-1}$ . The state of this dynamical system, at time  $t \in [t_j, t_{j+1})$ , is given by

$$v_t := S^{j+1}_{t-t_j} \circ S^j_{t_j-t_{j-1}} \circ \dots \circ S^1_{t_1-t_0}(v_0) . \quad (8)$$

Recall that a *part* of the closed convex cone  $V_{\geq 0}$  is an equivalence class for the relation  $\sim$  such that, for  $v, w \in V_{\geq 0}$ , we have  $v \sim w$  if and only if there exists two positive constants  $\alpha$  and  $\beta$  such that  $\alpha v \leq w \leq \beta v$ . A part is *trivial* if it is reduced to the equivalence class of the zero vector. *Hilbert’s projective metric*  $d_H$  is defined on every non-trivial part of  $V_{\geq 0}$  by the following formula

$$d_H(v, w) = \log \inf \left\{ \frac{\beta}{\alpha} : \alpha, \beta > 0, \alpha v \leq w \leq \beta v \right\} .$$

The infimum is achieved, since  $V_{\geq 0}$  is closed. The map  $d_H$  is nonnegative, it satisfies the triangular inequality, and  $d_H(v, w)$  vanishes if, and only if,  $v$  and  $w$  are proportional – this justifies the term “projective metric”. This metric plays a fundamental role in Perron–Frobenius theory and in metric geometry, and also in tropical geometry, see [19, 23, 6] for background.

When  $V_{\geq 0} = (\mathbb{R}_{\geq 0})^n$  is the standard orthant, and when all the entries of the vectors  $v$  and  $w$  are positive, we have

$$d_H(v, w) = \max_{k \in [n]} (\log v_k - \log w_k) - \min_{k \in [n]} (\log v_k - \log w_k) .$$

Denoting by  $e$  the unit vector of  $\mathbb{R}^n$ , we observe that

$$d_H(v, w) = \|\log v - \log w\|_H$$

where the notation  $\log v$  is understood entrywise, and

$$\|z\|_H = 2 \min_{c \in \mathbb{R}} \|x - ce\|_{\infty} .$$

In other words, up to a logarithmic change of variables,  $d_H$  arises by modding out the normed space  $(\mathbb{R}^n, \|\cdot\|_{\infty})$  by the one-dimensional space  $\mathbb{R}e$ .

We shall suppose that every semigroup  $S^i$  has an eigenvector  $u^i \geq 0$ , with eigenvalue  $\lambda^i$ , meaning that

$$S_t^i u^i = \exp(\lambda^i t) u^i, \quad \forall t \geq 0 .$$

Since  $S_t^i$  preserves  $V_{\geq 0}$ , this entails that  $\lambda^i$  is real.

We choose a linear form  $\varphi \in V'$  which we require to take nonnegative values on  $V_{\geq 0}$ . We shall think of  $V$  has the *state space* and  $\varphi$  as an *observable*. We consider the following scalar observation of the dynamics

$$Y_t := \varphi(v_t) .$$

We shall assume, in addition, that  $\varphi$  does not vanish on  $v_t$ , for all  $t \geq 0$ . Then, we can define the image of the observation by the logarithmic map

$$y_t := \log Y_t, \quad \forall t \geq 0 .$$

The following result shows that the logarithm of the observation stays at finite distance from a piecewise linear map.

**Theorem 1.** *Suppose that the semigroups  $S^1, \dots, S^m$  are order preserving. Suppose in addition that the initial condition  $v_0$  and the eigenvectors  $u^1, \dots, u^m$  all lie in the same non-trivial part of  $V$ , and that the linear form  $\varphi$  takes positive values on this part. Then, there exists a constant  $C$  such that the piecewise linear map  $t \mapsto y_t^{\text{trop}}$  defined, for  $t \in [t_j, t_{j+1})$ , by*

$$y_t^{\text{trop}} := \lambda_{j+1}(t - t_j) + \lambda_j(t_j - t_{j-1}) + \dots + \lambda_1(t_1 - t_0) + C ,$$

satisfies

$$|y_t - y_t^{\text{trop}}| \leq \frac{\Delta}{2}, \quad \forall t \geq 0 ,$$

where

$$\Delta = d_H(v_0, u^1) + d_H(u^1, u^2) + \dots + d_H(u^{m-1}, u^m) .$$

*Proof.* By definition of Hilbert’s projective metric, we can find positive constants  $\alpha_0, \beta_0$ , such that  $\alpha_0 u^1 \leq v_0 \leq \beta_0 u^1$  and  $d_H(v_0, u^1) = \log(\beta_0/\alpha_0)$ . Similarly, for all  $i \in [m-1]$ , we can find positive constants  $\alpha_i, \beta_i$ , such that  $\alpha_i u^{i+1} \leq u^i \leq \beta_i u^{i+1}$ , and  $d_H(u^i, u^{i+1}) = \log(\beta_i/\alpha_i)$ . For all  $j \geq 0$ , with  $j \leq m-1$ , and for all  $t \in [t_j, t_{j+1})$ , we set

$$z_t := \lambda_{j+1}(t - t_j) + \lambda_j(t_j - t_{j-1}) + \dots + \lambda_1(t_1 - t_0) .$$

Since the semigroups  $S^i$  are linear and order preserving, we prove by induction

$$\exp(z_t)\alpha_j \dots \alpha_0 u^{j+1} \leq v_t \leq \exp(z_t)\beta_j \dots \beta_0 u^{j+1} .$$

We observe that

$$\alpha_{m-1} \dots \alpha_{j+1} u^m \leq u^{j+1} \leq \beta_{m-1} \dots \beta_{j+1} u^m$$

and so

$$\exp(z_t)\alpha_{m-1} \dots \alpha_0 u^m \leq v_t \leq \exp(z_t)\beta_{m-1} \dots \beta_0 u^m .$$

Applying the linear form  $\varphi$  to latter inequalities, taking the image by the log map, and setting

$$C := \log \varphi(u^m) + \frac{1}{2} \sum_{j=0}^{m-1} \log(\beta_j \alpha_j) ,$$

we arrive at the bound of the theorem. □

A general principle from tropical geometry states that using “logarithmic glasses” reveals a piecewise linear structure [27, 14]. Theorem 1 is inspired by this principle. This motivates the notation  $y^{\text{trop}}$ , for the “tropicalization” of the logarithm of the observable  $Y$ .

Theorem 1 applies in particular to the transport model (5). We make Assumptions 1 and 2. Then the evolution operator of the system (5) preserves the space  $V = L^1([0, x_E^*]) \times L^1([0, x_I^*])$ . Moreover, when  $\alpha$  is constant, the eigenproblem (6) has a positive and continuous solution  $\bar{n}$ , with a real eigenvalue  $\lambda$ . Different stages of sanitary policies correspond to successive values  $\alpha_1, \dots, \alpha_m$  of  $\alpha(t)$ , leading to different semigroups  $S^i$ ,  $i \in [m]$ . Then, the solution  $v_t := n(\cdot, t)$  of (5) is determined as in (8). Each semigroup  $S^i$  yields a continuous and positive eigenvector  $u^i := \bar{n}^i$  satisfying (6) associated with a real eigenvalue  $\lambda^i$  of  $S^i$ . Continuous and positive functions defined on a compact interval are always in the same part of the cone of nonnegative functions of  $V$ , so Theorem 1 applies to this model.

Moreover, in the present situation, we can obtain an explicit estimate for the Hilbert projective distances between eigenvectors, arising in Theorem 1, by integrating the differential equations (6).

**Proposition 1.** *Suppose that Assumptions 1 and 2 hold, and that for  $i = 1, 2$ ,  $(\lambda^i, \bar{n}^i)$  is the solution  $(\lambda, \bar{n})$  of (6) when  $\alpha = \alpha_i$ . Then, we have*

$$d_H(\bar{n}^1, \bar{n}^2) \leq |\lambda_1 - \lambda_2|(x_E^* + x_I^*) .$$

The proof is immediate. Note that  $x_E^* + x_I^*$  corresponds to the maximal time between infection and end of infectiousity.

Theorem 1 carries over to discrete time systems in a straightforward manner.

## 9 Short term predictions

We now describe the basic methodology we propose to build confidence intervals for future occurrences of medical events related to epidemic progression, and raise alarms about its potential resurgence. We first consider a single time series of numbers of event occurrences. We then describe how to consolidate several time series corresponding to distinct medical events in order to construct improved alarm criteria. The simpler case of least squares fitting is considered first, the more robust  $\ell_1$  alternative is described next.

**Time series for a single type of events:** Let  $X(1), \dots, X(n)$  be indices of days, and we aim to do a forecast based on observations made on these days. Typically, on day  $d_0$ , we may select  $n = 7$  and let  $X(1) = d_0 - n, \dots, X(n) = d_0 - 1$  to perform a forecast on the basis of the last seven days. Let  $Y(t)$  denote the count of medical events (for instance, dispatches of ambulances) on day  $X(t)$ , and let  $Z(t) = \log Y(t)$ . Based on the previous discussion (epidemiological modeling) we assume that for all  $t = 1, \dots, n$ ,

$$Z(t) = \alpha + \beta X(t) + \epsilon_t$$

for constants  $\alpha, \beta$ , where  $\epsilon_t$  denotes some random noise. For simplicity we assume here i.i.d. noise sequence  $\epsilon_1, \dots, \epsilon_n$ , and that each  $\epsilon_t$  admits a Gaussian distribution  $\mathcal{N}(0, \sigma^2)$  with zero mean and variance  $\sigma^2$ .

Least-square estimates for the parameters  $\alpha, \beta$  are then provided by

$$\hat{\beta} = \frac{\sum_{t=1}^n (X(t) - \bar{X})(Z(t) - \bar{Z})}{\sum_{t=1}^n (X(t) - \bar{X})^2}, \quad \hat{\alpha} = \bar{Z} - \hat{\beta} \bar{X}, \quad (9)$$

where

$$\bar{X} = \frac{1}{n} \sum_{t=1}^n X(t), \quad \bar{Z} = \frac{1}{n} \sum_{t=1}^n Z(t). \quad (10)$$

The variance  $\sigma^2$  can be estimated as

$$\hat{\sigma}^2 = \frac{1}{n-2} \sum_{t=1}^n (Z(t) - \hat{Z}(t))^2, \quad (11)$$

where

$$\hat{Z}(t) := \hat{\alpha} + \hat{\beta} X(t). \quad (12)$$

Under the assumptions of i.i.d. Gaussian errors  $\epsilon_t$ , we have that, for each  $t$  corresponding to a future day  $X(t)$  (in particular,  $t \notin \{1, \dots, n\}$ ), the three following variables:

$$\frac{\hat{\alpha} - \alpha}{\hat{\sigma} \sqrt{\frac{1}{n} + \frac{\bar{X}^2}{\sum_{t'=1}^n (X(t') - \bar{X})^2}}}, \quad \frac{\hat{\beta} - \beta}{\hat{\sigma} \sqrt{\frac{1}{\sum_{t'=1}^n (X(t') - \bar{X})^2}}}, \quad \frac{Z(t) - \hat{Z}(t)}{\hat{\sigma} \sqrt{1 + \frac{1}{n} + \frac{(X(t) - \bar{X})^2}{\sum_{t'=1}^n (X(t') - \bar{X})^2}}},$$

all admit a bilateral Student distribution with  $n - 2$  degrees of freedom (see [15, Ch. 28] or [7]). Denote by  $t_{\gamma}^{n-2}$  the  $\gamma$ -th quantile of this distribution. For  $\epsilon \in [0, 1]$ , this provides us with the following confidence intervals with confidence  $1 - \epsilon$ :

$$\begin{aligned} \alpha &\in \left[ \hat{\alpha} - \hat{\sigma} \sqrt{\frac{1}{n} + \frac{\bar{X}^2}{\sum_{t'=1}^n (X(t') - \bar{X})^2}} t_{1-\epsilon/2}^{n-2}, \hat{\alpha} + \hat{\sigma} \sqrt{\frac{1}{n} + \frac{\bar{X}^2}{\sum_{t'=1}^n (X(t') - \bar{X})^2}} t_{1-\epsilon/2}^{n-2} \right], \\ \beta &\in \left[ \hat{\beta} - \hat{\sigma} \sqrt{\frac{1}{\sum_{t'=1}^n (X(t') - \bar{X})^2}} t_{1-\epsilon/2}^{n-2}, \hat{\beta} + \hat{\sigma} \sqrt{\frac{1}{\sum_{t'=1}^n (X(t') - \bar{X})^2}} t_{1-\epsilon/2}^{n-2} \right] \\ Z(t) &\in \left[ \hat{Z}(t) - \hat{\sigma} \sqrt{1 + \frac{1}{n} + \frac{(X(t) - \bar{X})^2}{\sum_{t'=1}^n (X(t') - \bar{X})^2}} t_{1-\epsilon/2}^{n-2}, \hat{Z}(t) + \hat{\sigma} \sqrt{1 + \frac{1}{n} + \frac{(X(t) - \bar{X})^2}{\sum_{t'=1}^n (X(t') - \bar{X})^2}} t_{1-\epsilon/2}^{n-2} \right] \end{aligned} \quad (13)$$

As an illustration, for  $n = 7$  and  $\epsilon = 5\%$ , we can plug in  $t_{0.975}^5 = 2.571$  in the last interval, and thus obtain a 95%-confidence interval centered around  $\hat{Z}(t)$  for  $Z(t) = \log Y(t)$ , the logarithm of the count  $Y(t)$  on a future day  $X(t)$ , that is:

$$Z(t) \in \left[ \hat{Y}(t) - 2.571 \times \hat{\sigma} \sqrt{1 + \frac{1}{n} + \frac{(X(t) - \bar{X})^2}{\sum_{t'=1}^n (X(t') - \bar{X})^2}}, \hat{Z}(t) + 2.571 \times \hat{\sigma} \sqrt{1 + \frac{1}{n} + \frac{(X(t) - \bar{X})^2}{\sum_{t'=1}^n (X(t') - \bar{X})^2}} \right] \quad (14)$$

Although we could extend this definition of the confidence interval for the short terms predictions of the value of  $Z(t)$ , we propose a more conservative confidence domain, in the shape of a trapezoid. It is obtained

by extending the upper-bound  $Z(t)^+$  (resp. the lower bound  $Z(t)^-$  of the 95% confidence interval on  $Z(t)$  by a line with slope equal to the upper-bound  $\beta^+$  (resp. lower-bound  $\beta^-$ ) of 95% confidence interval on  $\beta$ . For a given day  $t$ , the upper and lower envelopes of the trapezoid have ordinates

$$\left(\hat{\beta}(t - t_n) + \hat{Z}_n\right) \pm \left(\sqrt{\text{Var}(\hat{\beta})(t - t_n)} + \sqrt{\hat{\sigma}^2 + \text{Var}(\hat{Z}_n)}\right) t_{1-\epsilon/2}^{n-2}.$$

If instead of the count  $Y(t)$  on a particular day  $X(t)$ , we are interested in the trend of the epidemics, whether exploding or contracting, we should then consider the confidence interval for parameter  $\beta$ . Again for  $n = 7$  and  $\epsilon = 5\%$  this gives

$$\beta \in \left[\hat{\beta} - 2.571 \times \hat{\sigma} \sqrt{\frac{1}{\sum_{t'=1}^n (X(t') - \bar{X})^2}}, \hat{\beta} + 2.571 \times \hat{\sigma} \sqrt{\frac{1}{\sum_{t'=1}^n (X(t') - \bar{X})^2}}\right] \quad (15)$$

One-sided confidence intervals may also be provided, and are in fact more natural for the definition of alarm indicators.

For concreteness, assume we want to raise an alarm when the doubling time,  $\delta = (\log 2)/\beta$ , is  $\delta^*$  days or less, where  $\delta^*$  could be 10 for instance. This is equivalent to  $\beta$  exceeding  $(\log 2)/\delta^*$ . Thus  $\delta$  is less than  $\delta^*$  days with confidence  $1 - \epsilon$  when

$$\frac{\log 2}{\delta^*} < \hat{\beta} - t_{1-\epsilon}^{n-2} \sqrt{V},$$

where

$$V = \hat{\sigma} \sqrt{\frac{1}{\sum_{t'=1}^n (X(t') - \bar{X})^2}}.$$

Raising an alarm under this condition then amounts to calibrating the false positive probability at  $\epsilon$ . For instance, for  $\epsilon = 5\%$ , and  $n = 7$ , we would plug in  $t_{0.95}^7 = 2.015$  in the above expression.

Alternatively, raising an alarm under the condition

$$\frac{\log 2}{\delta^*} < \hat{\beta} + t_{1-\epsilon}^{n-2} \sqrt{V},$$

corresponds to calibrating the false negative probability (probability of not raising an alarm while  $\delta \leq 10$ ) at  $\epsilon$ .

Our alarm indicators correspond to the first choice, i.e. calibration of a false positive rate, with  $\delta^*$  set to  $+\infty$ .

**Alarm indicators based on multiple types of events:** Assume that several types  $j$  of events are available, and let  $J$  denote the corresponding set of events. For instance, we could distinguish between dispatches of ambulances bringing patients to Intensive Care Units as opposed to Non-intensive Care Units, thereby producing two distinct time series. Let  $X_j(t)$ ,  $t = 1, \dots, n_j$  denote the days on which counts  $Y_j(t)$  of type  $j$  event occurrences are to be used. Let  $Z_j(t) = \log Y_j(t)$ . We assume as before the linear regression model

$$Z_j(t) = \alpha_j + \beta_j X_j(t) + \epsilon_j(t), \quad t = 1, \dots, n_j.$$

Now for each of these times series, we can produce, based on the previous discussion, the estimator

$$\hat{\beta}_j := \frac{\sum_{t=1}^{n_j} (X_j(t) - \bar{X}_j)(Z_j(t) - \bar{Z}_j)}{\sum_{t=1}^{n_j} (X_j(t) - \bar{X}_j)^2},$$

where

$$\bar{X}_j = \frac{1}{n_j} \sum_{t=1}^{n_j} X_j(t), \quad \bar{Z}_j = \frac{1}{n_j} \sum_{t=1}^{n_j} Z_j(t).$$

Suppose in addition that the noise terms  $\epsilon_j(t)$  are mutually independent, Gaussian, with zero mean and variance  $\sigma_j^2$  for errors  $\epsilon_j(t)$ . Suppose finally that the exponents  $\beta_j$  all coincide with  $\beta$ , the exponent that is characteristic of the epidemics progression. Denote by

$$V_j := \hat{\sigma}_j^2 \sqrt{\frac{1}{\sum_{t=1}^{n_j} (X_j(t) - \bar{X}_j)^2}}, \quad (16)$$

where, reproducing the computations for a single time series, we let

$$\hat{\sigma}_j^2 := \frac{1}{n_j - 2} \sum_{t=1}^{n_j} (Z_j(t) - \hat{Z}_j(t))^2,$$

and

$$\hat{Z}_j(t) := \hat{\alpha}_j + \hat{\beta}_j X_j(t).$$

As previously,  $V_j$  is our estimate of the variance of estimate  $\hat{\beta}_j$ . We finally propose to combine the individual estimators  $\hat{\beta}_j$  into

$$\hat{\beta} := \frac{\sum_{j \in J} \frac{1}{V_j} \hat{\beta}_j}{\sum_{j \in J} \frac{1}{V_j}}. \quad (17)$$

For the sake of simplicity, let us approximate the bilateral Student distribution with  $n - 2$  degrees of freedom by the standard distribution  $\mathcal{N}(0, 1)$ . We then have the approximate distributions  $\hat{\beta}_j \approx \mathcal{N}(\beta, V_j)$ , and hence the approximate distribution  $\hat{\beta} - \beta \approx \mathcal{N}(0, V)$ ,

$$V := \frac{1}{\sum_{j \in J} \frac{1}{V_j}}. \quad (18)$$

Weighing the individual estimators  $\hat{\beta}_j$  by the reciprocal of their variances as just done minimizes the variance of the resulting estimator. The same approach as previously considered then leads to the following conditions for alarm raising:

To raise an alarm when the doubling time  $\delta = (\log 2)/\beta$  exceeds  $\delta^*$  days (e.g.,  $\delta^* = 10$ ), if we target a false alarm probability of  $\epsilon$ , we are led to raise an alarm when Condition

$$\frac{\log 2}{\delta^*} < \hat{\beta} - g_{1-\epsilon} \sqrt{V}, \quad (19)$$

where  $g_{1-\epsilon}$  is the  $1 - \epsilon$ -quantile of the standard Gaussian distribution.

If instead we target a false negative probability (probability of not raising an alarm) at  $\epsilon$ , we would then raise an alarm when

$$\frac{\log 2}{\delta^*} < \hat{\beta} + g_{1-\epsilon} \sqrt{V}, \quad (20)$$

**More robust  $\ell_1$ -based approach:** The previous estimators and derived alarm conditions have the appeal of simplicity, but can be advantageously replaced by more robust versions, that are less sensitive to the presence of outliers.

A popular alternative is the following  $\ell_1$  criterion. We again consider  $Z_j(t) := \log Y_j(t)$ , where  $Y_j(t)$  is the number of type  $j$  events on day  $X_j(t)$ . We then let  $\hat{\alpha}_j, \hat{\beta}_j$  achieve the minimum of the criterion  $\sum_{t=1}^{n_j} |\alpha_j + \beta_j X_t^j - Y_t^j|$ . They are obtained by solving a linear program. Here we assume that observations  $Z_j(t)$  are mutually independent and distributed according to density  $f_{j,t}(z) = \frac{1}{2\lambda_j} \exp(-|z - \alpha_j - \beta_j X_j(t)|/\lambda_j)$ . In other words this corresponds to adding a Laplace observation noise with density  $\frac{1}{2\lambda_j} \exp(-|z|/\lambda_j)$  to the signal of interest  $\alpha_j + X_j(t)\beta_j$ . The above  $\ell_1$  minimization criterion corresponds to maximum likelihood estimation of  $\alpha_j, \beta_j$  in this observational noise model, as its log-likelihood is given by

$$-|T| \log(2\lambda_j) - \sum_{t=1}^{n_j} \frac{|Z_j(t) - \alpha_j - \beta_j X_j(t)|}{\lambda_j}.$$

A rich theory for the performance of the resulting estimators is available, see for instance [16]. [16] treat general i.i.d. errors, and do not restrict themselves to e.g. Laplacian distribution of errors; recent work like [26] experiments techniques to obtain confidence intervals when distribution of errors is unknown. Here we make the choice of Laplace-distributed errors for sake of simplicity. In particular, the asymptotic theory in [16] suggests the approximation

$$\hat{\beta}_j \sim \mathcal{N}(\beta_j, V_j)$$

where

$$\hat{\lambda}_j := \frac{1}{n_j} \sum_{t=1}^{n_j} |Z_j(t) - \hat{\alpha}_j - \hat{\beta}_j X_j(t)|, \quad (21)$$

and

$$V_j := (\hat{\lambda}_j)^2 \frac{1}{\sum_{t=1}^{n_j} X_j(t)^2 - \frac{1}{n_j} (\sum_{t=1}^{n_j} X_j(t))^2}. \quad (22)$$

We again consider that multiple types  $j \in J$  of time series are conjointly available, and that each  $\beta^j$  coincides with  $\beta$ , the parameter to be estimated. Assuming the  $\hat{\beta}_j$  to be independent with  $\hat{\beta} \sim \mathcal{N}(\beta, V)$ , leads us to define the estimator

$$\hat{\beta} := \frac{\sum_{j \in J} \frac{\hat{\beta}_j}{(\hat{\lambda}_j)^2}}{\sum_{j \in J} \frac{1}{(\hat{\lambda}_j)^2}}, \quad (23)$$

whose distribution is then given by  $\hat{\beta} \sim \mathcal{N}(\beta, V)$  where

$$V = \frac{1}{\sum_{j \in J} \frac{\sum_{t=1}^{n_j} X_j(t)^2 - (\sum_{t=1}^{n_j} X_j(t))^2 / n_j}{(\hat{\lambda}_j)^2}}. \quad (24)$$

A symmetric  $(1 - \epsilon)$ -confidence interval for  $\beta$  is then provided by

$$\beta \in I := \left[ \hat{\beta} - g_{1-\epsilon/2} \sqrt{V}, \hat{\beta} + g_{1-\epsilon/2} \sqrt{V} \right]. \quad (25)$$

Similarly,  $(1 - \epsilon)$ -confidence one-sided intervals for  $\beta$  are obtained by letting

$$\beta \in I' := [\hat{\beta} - g_{1-\epsilon} \sqrt{V}, +\infty), \quad \beta \in I'' := (-\infty, \hat{\beta} + g_{1-\epsilon} \sqrt{V}]. \quad (26)$$

The doubling time  $\delta$  is given by  $(\log 2)/\beta$  if  $\beta > 0$ , and  $+\infty$  otherwise. This gives the  $1 - \epsilon$ -confidence conditions for  $\delta$ :

$$\text{if } \hat{\beta} - g_{1-\epsilon} \sqrt{V} > 0, \quad \delta \in I_1 = \left[ 0, \frac{\log 2}{\hat{\beta} - g_{1-\epsilon} \sqrt{V}} \right], \quad (27)$$

and

$$\delta \in I_2 = \left[ \frac{\log 2}{\max(0, \hat{\beta} + g_{1-\epsilon} \sqrt{V})}, +\infty \right). \quad (28)$$

For concreteness assume we want to raise an alarm when  $\delta$  is  $\delta^*$  days or less, where  $\delta^*$  could be 10. From the above consideration,  $\delta$  is below  $\delta^*$  days with confidence  $1 - \epsilon$  when

$$\frac{\log 2}{\delta^*} < \hat{\beta} - g_{1-\epsilon} \sqrt{V}.$$

Raising an alarm under this condition then amounts to calibrating the false positive probability at  $\epsilon$ .

Alternatively, we may consider to raise an alarm under the condition

$$\frac{\log 2}{\delta^*} < \hat{\beta} + g_{1-\epsilon} \sqrt{V}.$$

This would correspond to calibrating the false negative probability (probability of not raising an alarm while  $\delta \leq \delta^*$ ) at  $\epsilon$ .

## 10 Conclusion

We have shown that monitoring of emergency calls to EMS allows to anticipate the evolution of an epidemic by providing several signals, each with specific characteristics in terms of time lag and reliability.

Our study illustrates the spatially differentiated nature of the epidemic kinetics, with significant doubling time differences between neighboring departments.

Such spatial differentiation, if present at a granularity finer than that of departments considered here, could be exploited using the methods described in the present work in order to detect potential epidemic resurgences at the corresponding spatial granularity. This shows great promise in enabling detection of so-called epidemic clusters.

There is thus huge potential in the extension of this work and its application to finer spatial resolution.

Notwithstanding such extensions, monitoring epidemic kinetics through EMS calls at regional levels can already be exploited to define region-specific sanitary measures, such as lifting of travel bans, proportionate to the regional situation, and to allow early detection of epidemic resurgence. Importantly, we expect this finding to be applicable in full generality to EMS organizations worldwide. Thus the methods introduced here may be of wide applicability to combat Covid-19. Beyond Covid-19, EMS organizations have a unique role to play in early detection of sanitary crises.

## 11 Acknowledgments

We thank the operational team of DSI of AP-HP, who helped to extract information records, especially Stéphane Crézé, Laurent Fontaine, Pierre Cabot, François Planeix, Fabrice Tordjman, Grégory Terrell and Martine Spiegelmann.

We thank Pr. Renaud Piarroux for very helpful remarks. We thank Pr. Bruno Riou for his suggestion to include quantitative statistical estimates in the present article. We thank Pr. Frédéric Batteux for having provided epidemiological information. We thank Dr. François Braun (SAMU 57) and Dr. Vincent Bounes (SAMU 31) for providing comparison elements between their departments. We thank Dr. Nicolas Poirot for introducing us to SAMU 31. We thank Dr. Paul-Georges Reuter (SAMU 92) for useful comments on the interpretation of SAMU data relative to the Covid crisis.

We thank Ayoub Foussoul, for having developed a robust dynamic programming algorithm, allowing one to consolidate the results of this manuscript concerning the best piecewise linear approximation of the log of observables. We thank Jérôme Bolte, for providing insights on non-convex and non-smooth best-approximation problems.

We thank Tania Lasisz for her help in the administration of the project, and Guillermo Andrade Barroso, Thomas Calmant and Matthieu Simonin for their contribution to software development.

We thank NXO France Integrator of communication solutions team and SIS Centaure15 solution from GFI World team for the help they provided and their availability for the project.

We thank Orange Flux Vision (especially Jean-Michel Contet) for having provided daily population estimates, at the scale of the department, helping to calibrate our models.

We thank Enedis (especially Pierre Gotelaere and his team) for having provided an estimation of the departure rate of households, aggregated at the scale of departments and districts, helping us to refine our model.

We thank SFR Geostatistic Team (especially Loic Lelièvre) for having provided estimates of flows between Paris and province, aggregated at the scale of departments and districts, allowing us to incorporate mobility in our model.

Stéphane Gaubert thanks Nicolas Bacaër for a decisive help, concerning epidemiological and mathematical analysis, provided during the week of March 16th-20th. He thanks Cormac Walsh for improvements of the text. He also thanks Thomas Lepoutre.

The INRIA-École polytechnique team thanks the Direction de Programme de la Plate Forme d'Appels d'Urgences - PFAU at Préfecture de Police, DOSTL (Régis Reboul), and Brigade de Sapeurs Pompiers de



Paris (especially Gen. Jean-Marie Gontier and Capt. Denis Daviaud) for having provided precious elements of comparison concerning the calls received at the emergency numbers 17-18-112.

## References

- [1] N. Bacaer. Un modèle mathématique des débuts de l'épidémie de coronavirus en France. hal-02509142, 2020.
- [2] David J Baker, Caroline Telion, and Pierre Carli. Multiple casualty incidents: the prehospital role of the anesthesiologist in europe. *Anesthesiology clinics*, 25(1):179–188, 2007.
- [3] A. Berman and R.J. Plemmons. *Nonnegative matrices in the mathematical sciences*. Academic Press, 1979.
- [4] G. C. Calafiore, S. Gaubert, and C. Possieri. Log-sum-exp neural networks and posynomial models for convex and log-log-convex data. *IEEE Transactions on Neural Networks and Learning Systems*, 31(3):827–838, 2020.
- [5] Yi-Cheng Chen, Ping-En Lu, Cheng-Shang Chang, and Tzu-Hsuan Liu. A time-dependent sir model for covid-19 with undetectable infected persons. 2020. [http://gibbs1.ee.nthu.edu.tw/A\\_TIME\\_DEPENDENT\\_SIR\\_MODEL\\_FOR\\_COVID\\_19.PDF](http://gibbs1.ee.nthu.edu.tw/A_TIME_DEPENDENT_SIR_MODEL_FOR_COVID_19.PDF).
- [6] G. Cohen, S. Gaubert, and J.-P. Quadrat. Duality and separation theorems in idempotent semimodules. *Linear Algebra and Appl.*, 379:395–422, 2004.
- [7] Harald Cramér. *Mathematical methods of statistics*, volume 43. Princeton university press, 1999.
- [8] Agence Régionale de Santé Grand Est. Coronavirus covid 19 en grand est: Point de situation. Press release of March 8<sup>th</sup>, available from [https://www.grand-est.ars.sante.fr/system/files/2020-03/Covid19\\_point\\_GrandEst080320.pdf](https://www.grand-est.ars.sante.fr/system/files/2020-03/Covid19_point_GrandEst080320.pdf), 2020.
- [9] Laura Di Domenico, Giulia Pullano, Chiara E. Sabbatini, Pierre-Yves Boëlle, and Vittoria Colizza. Expected impact of lockdown in Île-de-France and possible exit strategies. Report #9 , [www.epicx-lab.com/covid-19.html](http://www.epicx-lab.com/covid-19.html), 2020.
- [10] Santé Publique France. Données hospitalières relatives à l'épidémie de Covid-19, 2020. <https://www.data.gouv.fr/fr/datasets/donnees-hospitalieres-relatives-a-lepidemie-de-covid-19/>, Retrieved on May 10th, 2020.
- [11] Nikolaus Hansen and Andreas Ostermeier. Completely derandomized self-adaptation in evolution strategies. *Evolutionary Computation*, 9(2):159–195, 2001.
- [12] Martin Hirsch, Pierre Carli, Rémy Nizard, Bruno Riou, Barouyr Baroudjian, Thierry Baubet, Vibol Chhor, Charlotte Chollet-Xemard, Nicolas Dantchev, Nadia Fleury, et al. The medical response to multisite terrorist attacks in paris. *The Lancet*, 386(10012):2535–2538, 2015.
- [13] Insee. Ménages selon la taille en 2016. Comparaisons régionales et départementales, 2019. <https://www.insee.fr/fr/statistiques/2012714>.
- [14] I. Itenberg, G. Mikhalkin, and E. Shustin. *Tropical algebraic geometry*. Oberwolfach seminars. Birkhäuser, 2007.
- [15] Norman Lloyd Johnson, Samuel Kotz, and Narayanaswamy Balakrishnan. *Continuous univariate distributions*. Wiley, New York, 1994.
- [16] Roger W Koenker and Gilbert Bassett. Regression quantiles. *Econometrica*, 46(1):33–50, 1978.

- [17] J. C. Lagarias, J. A. Reeds, M. H. Wright, , and P. E. Wright. Convergence properties of the Nelder-Mead simplex method in low dimensions. *SIAM Journal of Optimization*, 9(1):112–147, 1998.
- [18] Stephen A. Lauer, Kyra H. Grantz, Qifang Bi, Forrest K. Jones, Qulu Zheng, Hannah R. Meredith, Andrew S. Azman, Nicholas G. Reich, and Justin Lessler. The incubation period of coronavirus disease 2019 (covid-19) from publicly reported confirmed cases: Estimation and application. *Annals of Internal Medicine*, 172(9):577–582, 2020. PMID: 32150748.
- [19] B. Lemmens and R. Nussbaum. *Nonlinear Perron-Frobenius Theory*, volume 189 of *Cambridge Tracts in Mathematics*. Cambridge University Press, May 2012.
- [20] Clément Massonnaud, Jonathan Roux, and Pascal Crépey. Covid-19: Forecasting short term hospital needs in France. Rapport disponible sur Sfar.org, 2020.
- [21] P. Michel, S. Mischler, and B. Perthame. General relative entropy inequality: an illustration on growth models. *J. Math. Pures et Appl.*, 84(9):1235–1260, May 11 2005.
- [22] S. Mischler and J. Scher. Spectral analysis of semigroups and growth-fragmentation equations. *Annales de l’Institut Henri Poincaré (C) Non Linear Analysis*, 33(3):849 – 898, 2016.
- [23] A. Papadopoulos and M. Troyanov. Weak Finsler structures and the Funk weak metric. *Math. Proc. Cambridge Philos. Soc.*, 147(2):419–437, 2009.
- [24] B. Perthame. *Transport equations in biology*. Birkhäuser, 2007.
- [25] Henrik Salje, Cécile Tran Kiem, Noémie Lefrancq, Noémie Courtejoie, Paolo Bosetti, Juliette Paireau, Alessio Andronico, Nathanaël Hoze, Jehanne Richet, Claire-Lise Dubost, Yann Le Strat, Justin Lessler, Daniel Bruhl, Arnaud Fontanet, Lulla Opatowski, Pierre-Yves Boëlle, and Simon Cauchemez. Estimating the burden of SARS-CoV-2 in France. *pasteur-02548181*, 2020.
- [26] Gabriela Stangenhaus, Subhash C Narula, and Ferreira F Pedro. Bootstrap confidence intervals for the minimum sum of absolute errors regression. *Journal of statistical computation and simulation*, 48(3-4):127–133, 1993.
- [27] O. Viro. Dequantization of real algebraic geometry on logarithmic paper. In *European Congress of Mathematics, Vol. I (Barcelona, 2000)*, volume 201 of *Progr. Math.*, pages 135–146. Birkhäuser, Basel, 2001.

## A Algorithms to compute a best approximation of the logarithm of the number of events by a piecewise linear map

As said, we aim to approximate  $\log Y_s(t)$  by a function  $\varphi(t) := \min_{1 \leq j \leq \nu} (\lambda_j t + c_j)$  where  $\nu$  is the number of phases with constant sanitary policy during the considered time period. The parameters  $\lambda_j, c_j$  are assumed without loss of generality to satisfy  $\lambda_1 \leq \lambda_2 \leq \dots \leq \lambda_\nu$ . The concavity constraint imposed on the approximating function  $\varphi(t)$  makes the problem different from standard function approximation problems, and contributes to the robustness of the fitting procedure by reducing the amount of overfitting.

The two most natural criteria for fitting function  $\varphi(t)$  to observations  $\log Y_s(t)$  are to minimize either a least squares, or  $\ell_2$  loss function  $\sum_t |\varphi(t) - \log Y_s(t)|^2$ , or an  $\ell_1$  loss function  $\sum_t |\varphi(t) - \log Y_s(t)|$ . As discussed in Section 9, the latter is more robust in being less sensitive to outliers, and is the one used on Figure 4.

The corresponding optimization problem over parameters  $\lambda_i, c_i$  is non-convex as soon as  $\nu \geq 2$ . A straightforward option is to use a derivative free procedure, like the Nelder-Mead [17] algorithm. Depending on the initial point, this algorithm may converge to a local minimum, which may not be epidemiologically significant. So, a possibility is to guide the algorithm by providing it a initial guess of the optimal solution. To do, we start by an a priori selection of the time periods over which function  $\varphi(t)$  is linear (which could

be obtained by prior knowledge of delay parameters  $\tau$  and times of policy changes, or found by brute force search). We then determine a minimum cost linear fit of target function  $\log Y_s(t)$  over each such period, and use the concave envelope of the resulting function as our initial condition for local search. This is how we initially obtained the best  $\ell_1$  approximation shown on Figure 4. We also used CMA-ES for comparison [11]. Both Nelder-Mead and CMA-ES algorithms appear to be sensitive to the initial conditions. Notice in this respect that the objective function is linear on the cells of a polyhedral complex and that it can be constant on certain unbounded cells of this complex, so a local search algorithm may be trapped in a cell in which the function is constant. Alternative approaches, leading to the global optimum, are under investigation. In particular, Ayoub Foussoul (École polytechnique) provided us with a dynamic programming solver, allowing us to certify the global optimality of the approximation shown in Figure 4, up to a small precision. Another perspective is to observe that this best approximation problem is equivalent to a “shallow” learning problem, looking for the parameters of a neural networks with a single hidden layer and min-type activation functions, see [4].